5

A Pseudopotential Viewpoint of the Electronic and Structural Properties of Crystals

ALEX ZUNGER

I. INTRODUCTION

In 1956, at the American Society of Metals meeting on alloy phases, J. C. Slater commented: "I don't understand why you metallurgists are so busy in working out experimentally the constitution of polynary metal systems. We know the structure of the atoms, we have laws of quantum mechanics, and we have calculating machines, which can solve the pertinent equations rather quickly" (Slater, 1956). Today, almost 25 years later, our computing ability has increased by two to three orders of magnitude, yet no complex alloy structure has been predicted by such a variational quantum-mechanical approach. At the same time, the semiclassical notions of Pauling, Hume-Rothery, Pearson, and others have continued to guide metallurgists, crystallographers, and crystal chemists in rationalizing even very complex crystal structures.

Our experience in understanding the occurrence of a large variety of crystal structures in nature has been traditionally expressed in two general frameworks: variational quantum mechanics and a semiclassical approach. The

Structure and Bonding in Crystals, Vol. I

ISBN 0-12-525101-7

bulk of our experience in understanding the structural properties of molecules and solids from the quantum-mechanical viewpoint is expressed in terms of constructs originating from the calculus of variation: total energy minimization, optimum subspaces of basis functions, etc. In this approach, one constructs a quantum mechanical energy functional representing the Born–Oppenheimer surface of a compound; its variational minimum in configuration space $\{\mathbf{R}\}$ is then sought, usually by first reducing the problem to a single-particle Schrödinger equation. The elementary constructs defining this energy functional—the interelectronic effective potential $V_{ee}(\mathbf{r}, \mathbf{r}')$ and the electron-core potential $V_{ec}(\mathbf{r}, \mathbf{R})$—can be treated at different levels of sophistication (e.g., semiempirical tight-binding, Thomas–Fermi, Hartree–Fock, density-functional, pseudopotential, etc.). Similarly, a number of choices exist for the wavefunction representation (e.g., the Bloch and molecular-orbital representations or the Wannier and valence-bond models, etc.). This approach has become increasingly refined recently, producing considerable detailed information and insight into the electronic structure of molecules (e.g., Schaefer, 1977a,b) and simple solids (e.g., Moruzzi *et al.*, 1978).

The semiclassical approach to crystal and molecular structure, on the other hand, involves the construction of phenomenological scales ("factors") on which various aspects of bonding and structural characteristics are measured. These include chemical, crystallographic, and metallurgical constructs, such as the electronegativity, the geometry and size factors, the coordination number factor, the average electron number factor, the orbital promotion energy factor, etc. (e.g., Pearson, 1969). These factors are then represented by various quantitative scales (bond order, elemental work function, ionic, metallic, and covalent radii, electronegativity scales, etc.) that are used to deductively systematize a variety of structural properties. Such intuitive and often heuristic scales have had enormous success in rationalizing a large body of chemical and structural phenomena, often in an ingenious way (Pauling, 1960; Hume-Rothery and Raynor, 1954; Pearson, 1972; Darken and Gurry, 1953; Miedema, 1976). More recently, these semiclassical scales have been used in *quantitative* models, such as the semiempirical valence force field method (Pawley, 1968; Warshel, 1977) and Miedema's heat of formation model (Miedema, 1973, 1976; Miedema *et al.*, 1975), where the remarkable predictive power of these approaches has been demonstrated over large data bases (literally hundreds of molecules and solids).

Even before the pioneering studies of Goldschmidt, Pauling, and others, it was known thermodynamically that the structure-determining energy ΔE_s of most ordered solids is small compared to the total cohesive energy ΔE_0. Measured heats of transformation and formation data (Hultgren *et al.*, 1973; Kubaschewski and Alcock, 1979), as well as quantum-mechanical

calculations of stable and hypothetical structures, indicate that $\Delta E_s/\Delta E_0$ can be as small as 10^{-3}–10^{-4}. This poses an acute difficulty for variational quantum-mechanical models. The elementary constructs of the quantum-mechanical approach $V_{ee}(\mathbf{r}, \mathbf{r}')$ and $V_{ec}(\mathbf{r}, \mathbf{R})$, are highly nonlinear functions of the individual atomic orbitals that interact to form the crystalline wavefunctions (due to both the operator nonlocality of $V_{ee} + V_{ec}$ and their self-consistent dependence on the system's wavefunctions). Consequently, the structural energies ΔE_s become analytically inseparable from the total energies ΔE_0. One is then faced with the situation that the complex *weak interactions*, responsible for stabilizing one crystal structure rather than another, are often masked by errors and uncertainties in the calculation of the *strong Coulombic interactions* in the total interaction potentials $V_{ee}(\mathbf{r}, \mathbf{r}')$ and $V_{ec}(\mathbf{r}, \mathbf{R})$. Even though ΔE_s can be calculated quantum-mechanically with the aid of large computers (for sufficiently simple systems), it is notable that the extent and complexity of the information included in $V_{ee}(\mathbf{r}, \mathbf{r}')$ and $V_{ec}(\mathbf{r}, \mathbf{R})$ far exceeds that required to characterize a crystal structure. For example, although the 12 transition metals Sc, Ti, V, Cr, Fe, Y, Zr, Nb, Mo, Hf, Ta, and W have distinctly different quantum-mechanical effective potentials and are characterized by systematically varying cohesive energies ΔE_0, all of them appear in the same body-centered cubic (bcc) crystal form as elemental metals. Hence, at present, the quantum-mechanical approach seems to lack the simple *transferability* of structural constructs from one system to the other, as well as the *physical transparency* required to assess the origin of structural regularities. The semiclassical approach, on the other hand, concentrates on the construction of physically simple and transferable coordinates that may systematize directly the trends underlying the structural energies ΔE_s. The major limitations of the semiclassical approach seem to lie in the occurrence of internal linear dependencies among the various structural factors (e.g., orbital electronegativity and orbital promotion energy), as well as in the appearance of a large number of crystalline structures placed within narrow domains of the phenomenological structural parameters (e.g., Mooser–Pearson plots for non-octet AB compounds or diagrams of the frequency of occurrence of a given structure versus average electron per atom ratio). Even so, the semiclassical approaches provide valuable insight into the problem because they point to the underlying importance of establishing system-invariant *energy scales* (e.g., electronegativity, promotion energy) as well as *length scales* (e.g., covalent, metallic, and ionic radii).

For the 50–60 nontransition-metal binary octet compounds, the problem of systematizing the five crystal structures (NaCl, CsCl, diamond, zinc blende, and wurtzite) has been solved through the use of the optical dielectric electronegativity concept of Phillips and Van Vechten (1970; also Phillips, 1970).

This concept diagrammatically displays periodic trends when transferable elemental coordinates are used. Such diagrammatic Pauling-esque approaches are extended here to include intermetallic transition-metal compounds (a total of 565 compounds).

In this paper, I show that the recently developed first-principles nonlocal atomic pseudopotentials provide nonempirical elementary energy and length scales. By using a dual and transferable coordinate system derived from these scales, one is able to topologically separate the crystal structures of 565 binary compounds (including simple and transition-metal atoms) with a surprising accuracy. At the same time, these quantum-mechanically derived pseudopotentials allow one to conveniently define the elementary constructs $V_{ee}(\mathbf{r}, \mathbf{r}')$ and $V_{ec}(\mathbf{r}, \mathbf{R})$ and use them in detailed electronic structure calculations for molecules, solids, and surfaces. As such, this approach may provide a step in bridging the gap between the quantum-mechanical and semiclassical approaches to electronic and crystal structure.

The theoretical prediction of stable crystal structures is given diagrammatically much as in Mooser–Pearson plots. We show that each element A in the periodic table is characterized by three core radii r_s^A, r_p^A, and r_d^A, which measure the effective size of the atomic cores as experienced by valence electrons with angular momentum $l = 0$, 1, and 2, respectively. These radii are derived in Sec. III from the pseudopotential theory and tabulated in Table I for 70 elements. For each binary compound AB, we then construct the dual coordinates $R_\pi^{AB} = |r_p^A - r_s^A| + |r_p^B - r_s^B|$ and $R_\sigma^{AB} = |(r_p^A + r_s^A) - (r_p^B + r_s^B)|$. On an R_π^{AB} vs. R_σ^{AB} plot, we then find that the different groups of crystal structures of the 565 binary compounds occupy different regions. If one lumps together some of the crystallographically related structures, the accuracy of this prediction is better than 93%. The radii given in Table I can be used to systematize and analyze a large number of structural properties of crystals.

The success of this approach in correctly predicting the structural regularities of as many as 565 binary compounds using elemental coordinates that pertain directly only to the s and p electrons (and only indirectly to the d electrons through the screening potential produced by them) presents a striking result: it suggests that the *structural part* ΔE_s of the cohesive energy may be dominated by the s–p electrons. This points to the possibility that, while the relatively localized d electrons determine both *central cell effects* (such as octahedral ligand field and Jahn–Teller stabilizations) and the regularities in the structure-insensitive cohesive energy ΔE_0 of crystalline and liquid alloys, the longer range s–p wavefunctions are responsible for stabilizing one complex space group arrangement rather than another. There is a striking resemblance between this result and the semiclassical ideas indicating a remarkable correlation between the stable crystal structure of transition-metal systems and the number of s and p electrons, put forward by Engel in

1939 (also 1967) and subsequently greatly refined by Brewer (1963, 1967, 1968; Brewer and Wengent, 1973). In the Engel–Brewer approach, the d electrons play an important but indirect role in determining the energy required for exciting the ground atomic configuration to one that has available for bonding a larger number of unpaired s and p electrons. The Engel–Brewer approach has enabled the extension of the Hume-Rothery rules to transition metal systems simply by counting only the contributions of s and p electrons, and at the same time it has explained the stabilities of the bcc, hcp (hexagonal close-packed), and fcc (face-centered cubic) structures of the 33 elemental transition metals, the effects of alloying in multicomponent phase diagrams, as well as pressure effects on crystal structure stabilities, phenomena yet to be tackled by variational quantum-mechanical approaches. These conclusions on the crucial *structural* roles played by the s and p coordinates should be contrasted with the contemporary quantum-mechanical resonant tight-binding approaches suggested first by Friedel (1969) for elemental transition metals and recently extended to compounds by Pettifor (1979), Varma (1979), and others. These approaches emphasize the exclusive role of d electrons in determining *cohesive properties*. This approach explains the periodic trends in ΔE_0 and the bcc–fcc structural transitions of both elemental and alloyed transition metal systems by considering changes in the one-electron d energy levels, assumed to have a rectangular density of states.

The plan of this paper is as follows: in Sec. II, we introduce the pseudopotential concept and show how it can be used in general to define atomic parameters that correlate with crystal structures. In Sec. III, we derive the first-principles atomic pseudopotentials within the density-functional theory of electronic structure. In Sec. IV, we then show how these atomic pseudopotentials can be used to define intrinsic core radii that correlate with a large number of electronic and structural properties of crystals. These radii are used to separate diagrammatically the stable crystal structure of 565 binary AB compounds.

II. PSEUDOPOTENTIALS AND STRUCTURAL SCALES

Although traditionally the inner core orbitals and the outer valence orbitals are often treated on an equal footing in variational calculations of the electronic structure of atoms, molecules, and solids, it was recognized quite early that a large number of bonding characteristics are rather insensitive to the details of the core states (Hellman, 1935a,b, 1936; Gombas, 1935, 1967; Fock *et al.*, 1940). This relative insensitivity is a manifestation of the fact that the interaction energies involved in chemical bond formation (10^{-1}–10 eV), banding in solids (1–25 eV), or scattering events near the

Fermi energy (10^{-2}–10^{-3} eV) are often much smaller than the energies associated with the polarization or overlap of core states. Hence, the core orbitals with their nearly spherical symmetry and high binding energies are nearly unresponsive to many of the scattering phenomena that determine "valence-like" properties. Many methods treating the quantum structure of bound electrons, nucleons, and general Fermions have consequently omitted any reference to the core states, variationally treating only "valence" states (Hückel, CNDO, tight-binding, Hubbard models, optical potentials in nuclear physics, effective potentials in Fermi-liquid theories, and field-theory models of the Lamb shift, empirical valence potentials in atomic physics, etc.). Clearly, however, if no constraints are placed, such a variational treatment will result in an unphysical lowering of the energy of the valence states into the empty core ("variational collapse"). Much of the empirical parametrization characteristic of such methods is implicitly directed to avoid such a pathology. It was first recognized however by Phillips and Kleinman (1959) that the price for reducing the orbital space to valence states alone can be represented by an additional nonlocal potential term (pseudopotential) in the Hamiltonian.

Although the pseudopotential concept has offered great insight into the nature of bonding states in polymers and solids (e.g., Phillips, 1973), its calculation in practical electronic structure application has generally been avoided (Cohen and Bergstresser, 1966; Brust, 1968; Cohen and Heine, 1970). Instead, it has been replaced by a local form with disposable parameters adjusted to fit selected sets of data (semiconductor band structures, Fermi surface of metals, atomic term values, etc.). Since the valence electronic energies near the Fermi level are determined (to within a constant) by relatively low-momentum transfer electron-core scattering events ($|q| \approx 2k_F$), it has been possible in the past to successfully describe the one-electron optical spectra and Fermi surface of many solids assuming core pseudopotentials that are truncated to include only small momentum components (i.e., smoothly varying in the core region in configuration space). The freedom offered by the insensitivity of the electronic band structure dispersion relation $\varepsilon_j(\mathbf{k})$ to the variations of the pseudopotential in the core region has been exploited to obtain empirical potentials converging rapidly in momentum space and hence amenable to electron-gas perturbative theories (Harrison, 1966) and plane-wave-based band structure calculations (Cohen and Heine, 1970; Brust, 1968).

These soft-core *empirical* pseudopotentials have produced the best fits to date for the observed semiconductor band structures (e.g., see Cohen and Bergstresser, 1966), and their descendants, the soft-core self-consistent pseudopotentials, have yielded the most detailed information on semiconductor surface states (e.g., see Appelbaum and Hamann, 1976). The insen-

sitivity of $\varepsilon_j(\mathbf{k})$ to the high-momentum components of the pseudopotential has prompted an enormous literature in which different forms for the potential have been suggested (empty cores, square wells, Gaussian-shaped, etc.). Since, however, these pseudopotentials were fitted predominantly to energy levels in atoms and solids (and were not constrained to produce physically correct wavefunctions) they often yielded systematic discrepancies with experiment or all-electron calculations of the bonding charge density in molecules and solids (Yang and Coppens, 1974; Harris and Jones, 1978; Hamann, 1979): while correctly predicting a build-up of covalent charge on the bonds, such empirical pseudopotentials incorrectly suggested a *bond-perpendicular* charge density, rather than a *bond-elongated* density as envisioned by Coulson and Pauling and subsequently measured experimentally and supported by more refined calculation (Zunger, 1980). Such discrepancies result from the fact that higher momentum components (e.g., $|q| \gtrsim 6k_F$ in crystalline silicon), not included in energy-level-fitted soft-core pseudopotentials, are of importance in determining the directional distribution of the bonding charge density. It is such systematic omissions which make the soft-core empirical potentials inappropriate for predicting stable structures. The striking success of the empirical pseudopotential is that it made it possible to reduce the informational content of the often complex electronic spectra of semiconductors to a few (usually three to five) nearly transferable elemental parameters (empirical pseudopotential form factors). The assumed locality of the pseudopotential, as well as its truncation to low-momentum components, however, has limited its chemical content to reflect predominantly the low-energy electronic excitation spectrum rather than explicit structural and chemical regularities.

Recently, Simons (1971a,b) and Simons and Bloch (1973) have observed that there exists at least one class of structurally significant empirical pseudopotentials containing *very high momentum components* (i.e., $|q| \gg 2k_F$, or hard-core pseudopotentials). The general form of a screened pseudopotential is:

$$V_{\text{eff}}^{(l)}(\mathbf{r}) = V_{\text{ps}}^{(l)}(\mathbf{r}) + V_{\text{scr}}[n(\mathbf{r})] \tag{1}$$

(We use a capital $V(\mathbf{r})$ to denote solid-state potentials, while $v(r)$ will denote atomic or ionic potentials.) Here $V_{\text{ps}}^{(l)}(\mathbf{r})$ is the bare pseudopotential acting on the lth angular momentum wavefunction component, and $V_{\text{scr}}[n(\mathbf{r})]$ is the Coulomb, exchange, and correlation screening due to the pseudo charge density $n(\mathbf{r})$. The conventional core attraction Coulomb term $-Z/r$ is replaced by an angular momentum-dependent and spatially varying effective charge $Z_{\text{eff}}^{(l)}(\mathbf{r}) = rV_{\text{ps}}^{(l)}(\mathbf{r})$, while $V_{\text{scr}}[n]$ continues to represent interelectronic (valence–valence) interactions. For the simple case of *one-electron ions*, chosen by Simons and Bloch, the screening potential reduces to zero. The

bare atomic pseudopotential $v_{ps}^{(l)}(r)$ was then assumed to take a simple hard-core form:

$$v_{eff}^{(l)}(r) = v_{ps}^{(l)}(r) = \frac{B_l}{r^2} - \frac{Z_v}{r} \tag{2}$$

where Z_v is the valence charge and the parameter B_l is adjusted such that the negative of the orbital energies ε_{nl} obtained from the pseudopotential equation

$$\{-\tfrac{1}{2}\nabla_r^2 + v_{eff}^{(l)}(r)\}\psi_{nl}(r) = \varepsilon_{nl}\psi_{nl}(r) \tag{3}$$

match the observed ionization energies of one-electron ions such as Be^{+1}, C^{+3}, O^{+5}, etc. These hard-core pseudopotentials are characterized by an orbital-dependent crossing point r_l^0 at which $v_{eff}^{(l)}(r_l^0) = 0$. These orbital radii then possess the same periodic trends underlying the observed single-electron ionization energies through the periodic table. The remarkable feature of these radii is that they form powerful structural indices, capable of systematizing the various crystal phases of the octet $A^N B^{8-N}$ nontransition-metal compounds (St. John and Bloch, 1979). Such structural plots have been extended by Machlin *et al.* (1977) very successfully to some 45 nonoctet (nontransition-metal) compounds. More details on this approach are available in the cited literature.

The realization that these empirical orbital radii are characteristic of the atomic cores, and as such are approximately transferable to atoms in various bonding situations, has led to the construction of a number of new phenomenological relations of the form $G = f(r_l^0)$, correlating physical observables G in *condensed phases* with the orbital radii of the constituent *free atoms*. Some examples of G are the elemental work functions, the melting points of binary compounds, and the Miedema coordinates treated by Chelikowsky and Phillips (1978). What has been realized is that the characteristics of an isolated atomic core, reflected in the spectroscopically determined l-dependent turning points r_l^0, contain the fundamental constructs describing structural regularities in polyatomic systems. This can be contrasted with phenomenological electronegativity scales that are based on observables pertaining to the polyatomic systems themselves, such as the thermochemical Pauling scale, the dielectric Phillips–Van Vechten scale, and the Walsh scale.

While one normally considers structural and bonding characteristics to be predominantly determined by the atomic valence orbitals, these are not amenable to an analysis that reveals structural regularities in a simple manner. For instance, the different chemistries associated with carbon and silicon compounds are not transparently reflected by contrasting the carbon 2s and 2p with the silicon 3s and 3p orbitals, simply because the qualitative

difference in their nodal structure precludes the construction of a simple quantitative scale. In the pseudopotential representation, the nodal valence orbitals are transformed into nodeless valence pseudo wavefunctions such that, for example, the relevant differences in the new carbon 2s and silicon 3s orbitals can be measured on a simple quantum mechanical scale. Such a scale is provided by the orbital radii. The chemically pertinent information of these nodeless valence orbitals is coded in the pseudopotential. By building into the simple pseudopotentials of Eq. (2) the experimentally observed regularities of the ionization energies in the periodic table, Simons, Bloch, Chelikowsky, and Phillips (e.g., Phillips, 1977, 1978) have achieved an orbital radii scale that deciphers this core code.

It is not surprising that, although the orbital radii have typical dimensions of the core states, they do reflect structural regularities characteristic of the outer valence orbitals. This should be contrasted with the classical definitions of ionic, tetrahedral, covalent, or metallic radii: these definitions attempt to reproduce observed bond distances as *sums of single-site radii.* This bond additivity constraint forces these radii to have dimensions typical of valence orbitals, and as such these radii depend on the chemical environment (ionicity, coordination number, valency, spin state, etc.) rather strongly (e.g., Shannon and Prewitt, 1969). Even so, these classical radii constitute a very important reduction in the informational degrees of freedom required to specify chemical bonds: using, typically, 5000 measured bond distances, one has deduced about 250 ionic radii. The orbital radii approach takes, however, a different viewpoint: it assumes that the valence properties that an atom will take in bonded situations are coded in its effective core. Using the orbital radii as the characteristic fingerprint of the atomic cores, one achieves a further reduction of the structural information to a single set of transferable elemental radii.

This empirical Simons–Bloch radii have, however, few obvious shortcomings. Since the general atomic pseudopotential $v_{\text{eff}}^{(l)}(\mathbf{r})$ of Eq. (1) can be reduced to a simple form with $v_{\text{scr}} = 0$ only for single-electron-stripped ions, the empirical Simons–Bloch orbital radii can only be invoked for atoms for which stripped-ion spectroscopic data exists. This excludes most transition elements, which form a wealth of interesting intermetallic structures. Yet, even so, the extraction of a bonding scale from data on ions that lack any valence–valence interactions (e.g., C^{+3} and O^{+5}, representing chemical affinities of neutral C and O) may distort the underlying chemical regularities. In addition, the restriction to single-electron species means that the post-transition-series atoms (e.g., Cu, Ag, Au or Zn, Cd, Hg) are treated as having only one and two valence electrons, respectively, much like the alkali and alkaline earth elements, respectively. However, the increase in melting points and heats of atomization and the decrease in nearest-neighbor distances in

going from Group IIB to IB metals (e.g., Zn → Cu, Cd → Ag, and Hg → Au), as compared with the *opposite trend* in going from Group IIA to IA metals (Ca → K, Sr → Rb, and Ba → Cs), completely eliminates any possibility of Cu, Ag, and Au having effectively a single-bonding electron. Similar indications on the extensive s–d and p–d hybridization are given by the large bulk of photoemission data on Cu and Ag halides (Goldman, 1977). In keeping with the single-valence-electron restriction, one is also forced to define the d-orbital coordinate of the post-transition elements from the lowest *unoccupied* rather than occupied d orbital (i.e., 4d for Cu and Zn, 5d for Ag and Cd). This may be reasonably faithful to the chemical tendencies of post-transition elements with sufficiently deep occupied d orbitals and sufficiently low unoccupied d orbitals (e.g., Br, Te, I), but it is questionable for the elements with occupied semi core d shells in the vicinity of the upper valence band (e.g., CdS and ZnS). These pathologies can be corrected by empirically adjusting the valence charge Z_v in Eq. (2) for these elements (A. N. Bloch, unpublished results, 1980). Finally, the simple pseudopotential of Eq. (2) is not suitable for electronic structure studies, as indicated by Andreoni *et al.* (1978, 1979), because the wavefunctions of Eq. (3) are severely distorted relative to true valence orbitals by the unphysically long-range r^{-2} tail (similarly, the total energy of a solid described by this potential is divergent!). This has been corrected by Andreoni *et al.* by replacing the long-range B_l/r^2 term in Eq. (2) with an $A_l \exp(-\gamma_l r/r^2)$ term, with the additional parameter γ_l fixed to fit the orbital maxima. This leads to a new set of renormalized orbital radii differing considerably from the Simons–Bloch set.

One is hence faced with the situation that the soft-core empirical pseudopotential (e.g., Cohen and Heine, 1970) can be used to successfully fit the low-energy electronic band structure of solids, but it lacks the structurally significant turning points [i.e., $v_{\text{eff}}(r) = 0$ only at $r = \infty$]; whereas the empirical Simons–Bloch potentials do not yield a quantitatively satisfactory description of the electronic structure but do yield the correct structural regularities. The approach that we have taken to remedy this situation is to construct a pseudopotential theory from first-principles. The first-principles approach allows for the regularities of energy levels and wavefunctions to be systematically built into the atomic pseudopotentials, without appealing to any experimental data. Because no resort is made to simple, single-electron models, transition elements can be treated as easily as other elements, without neglecting the interactions between valence electrons or assuming that the highest occupied d levels belong to a chemically passive core. Furthermore, since the bare pseudopotential $v_{\text{ps}}^{(l)}(r)$ and the screening $v_{\text{scr}}[n(r)]$ are described in terms of well-defined quantum-mechanical constructs (such as Coulomb, exchange, and correlation interactions, Pauli forces, and orthogonality

holes) both the failures and the successes of the theory could be appreciated. This defines a link between the semiclassical length scale and the quantum-mechanical approach to structure.

III. FIRST-PRINCIPLES DENSITY-FUNCTIONAL PSEUDOPOTENTIALS

A. Construction of Density-Functional Atomic Pseudopotentials

These section describes the construction of atomic pseudopotentials from the density-functional formalism (Hohenberg and Kohn, 1964; Kohn and Sham, 1965). These potentials were first derived by Topiol *et al.* (1977) and Zunger and Ratner (1978) and subsequently refined by Zunger and Cohen (1978b, 1979a,b). Technical details are given elsewhere (Zunger *et al.*, 1979b; Zunger and Ratner, 1978; Zunger and Cohen, 1978b, 1979b; Zunger, 1979).

We first start with the *all-electron* approach. Consider a many-electron system with an electronic density matrix $\rho(\mathbf{r}, \mathbf{r}')$ interacting with an external potential $V_{\text{ext}}(\mathbf{r})$. In the conventional all-electron (ae) approach, both the core (c) and valence (v) wavefunctions, $\psi_j^c(\mathbf{r})$ and $\psi_j^v(\mathbf{r})$, respectively, are treated on the same footing. The effective single-particle potential appearing in the Schrödinger equation is then written as a sum of the external potential and the interelectronic response (screening):

$$V_{\text{eff}}^{\text{ae}}(\mathbf{r}) = V_{\text{ext}}(\mathbf{r}) + V_{\text{scr}}^{\text{c,v}}[\rho(\mathbf{r}, \mathbf{r}')] \tag{4}$$

Here $V_{\text{scr}}^{\text{c,v}}[\rho(\mathbf{r}, \mathbf{r}')]$ is a functional of the total core plus valence charge density $\rho = \rho_c + \rho_v$ and includes the interelectronic Coulomb $V_{ee}[\rho]$ as well as exchange $V_x[\rho]$ and correlation $V_{cr}[\rho]$ terms. These screening terms take different forms in the Hartree–Fock and density-functional formalisms used here. The external potential $V_{\text{ext}}(\mathbf{r})$ may be identified in atoms with the electron-nuclear attraction term $-(Z_c + Z_v)/r$ (where Z_c and Z_v denote the number of core and valence electrons, respectively) or with the sum of the analogous terms and the Ewald ion–ion repulsion in infinite systems. The wavefunctions $\{\psi_j^{c,v}(\mathbf{r})\}$ of the all-electron Hamiltonian $H^{\text{ae}} = -\frac{1}{2}\nabla^2 + V_{\text{eff}}^{\text{ae}}$ have a nodal structure resulting from the orthogonality constraint. These form a basis for constructing the ground-state density matrix $\rho(\mathbf{r}, \mathbf{r}')$, which is then used to calculate self-consistently the screening potential as well as the ground-state total energy.

We now turn to the *pseudopotential* approach. In this representation, one seeks an effective potential $V_{\text{eff}}^{\text{ps}}$ that will produce in a variational Schrödinger equation the *valence* wavefunctions $\chi_j(\mathbf{r})$ and orbital energies λ_j as its lowest-lying solutions. As, by construction, no core states occur, $\chi_j(\mathbf{r})$ does not have

to be core-orthogonal and, hence, may be constructed as nodeless for each of the lowest angular symmetries. One therefore replaces the all-electron effective potential of Eq. (4) by the pseudopotential effective potential:

$$\begin{aligned} V_{\text{eff}}^{\text{ps}} &= V_{\text{ps}}(\mathbf{r}) + V_{\text{scr}}^{\text{v}}[n(\mathbf{r})] \\ &= [V_{\text{ext}}^{\text{v}}(\mathbf{r}) + W_{\text{R}}(\mathbf{r})] + V_{\text{scr}}^{\text{v}}[n(\mathbf{r})] \end{aligned} \tag{5}$$

where $V_{\text{ext}}^{\text{v}}$ is the valence-projected external potential [e.g., in an atom $-Z_{\text{v}}/r$ rather than $-(Z_{\text{v}} + Z_{\text{c}})/r$], $W_{\text{R}}(\mathbf{r})$ is the yet-unspecified repulsive part of the pseudopotential, and $V_{\text{scr}}^{\text{v}}[n(\mathbf{r})]$ is the screening due to the valence pseudo charge density $n(\mathbf{r}) = \sum_{\text{j}} \chi_{\text{j}}^{*}(r)\chi_{\text{j}}(r)$.

Instead of constructing $W_{\text{R}}(\mathbf{r})$ directly for the molecules or solids of interest, one attempts first to calculate this for simple model systems such as atoms. Then, the total pseudopotential $V_{\text{ps}}(\mathbf{r})$ for a general system will be approximated by superimposing the atomic pseudopotentials $v_{\text{ps}}^{(\text{l})}(r)$ over all atoms and angular momenta, i.e.,

$$V_{\text{ps}}^{(\text{l})}(\mathbf{r}) = \sum_{\mathbf{R}_{\text{n}}} v_{\text{ps}}^{(\text{l})}(\mathbf{r} - \mathbf{R}_{\text{n}})\hat{P}_{\text{l}}$$

where $\hat{P}_{\text{l}}$ is the angular momentum projection operator, and $\mathbf{R}_{\text{n}}$ is the position vector of atom n. To build into the atomic pseudopotentials an element of transferability, one needs to construct $v_{\text{ps}}^{(\text{l})}(r)$ such that its dependence on the chemical environment is minimal. Formally this amounts to minimizing the energy and quantum-state dependence of $v_{\text{ps}}^{(\text{l})}(r)$. The mathematical implications of this have been previously discussed (Zunger *et al.*, 1979). It will suffice here to say that such a minimization of the pseudopotential's energy and state dependence can be achieved by maximizing the spatial range (starting from $r = \infty$ and going inwards to a finite value $r = R_{\text{c}}$) of identity between the true valence orbital $\psi_{\text{nl}}^{\text{v}}(r)$ and the pseudo orbital $\chi_{\text{nl}}(r)$ and, at the same time, minimizing to the extent possible the amplitude and lowest derivatives of $\chi_{\text{nl}}(r)$ in the core region ($0 \leqslant r \leqslant R_{\text{c}}$). The formulation of *transferable* atomic pseudopotentials, through the imposition of certain physically motivated constrains on the pseudo wavefunctions, is central to the present approach. No such explicit considerations have been undertaken in the development of previous pseudopotentials.

To the extent that the construction of the pseudopotentials $V_{\text{ps}}^{(\text{l})}(\mathbf{r})$ can be made simple, the study of valence-related properties of solids through the solution of the *pseudopotential* single-particle problem is both computationally and conceptually simpler than that study via the solution of the *all-electron* problem. This relative simplicity is not only because the pseudopotential approach treats fewer ("reactive") electrons and permits nodeless and spatially smooth wavefunctions, but it is also because, to within a good approxi-

mation, the atomic pseudopotential can be constructed from nearly system-invariant transferable quantities. Such transferable atomic pseudopotentials $v_{ps}^{(l)}(r)$ can then be used, through Eq. (5), to construct self-consistently the effective potential for arbitrary molecules and solids and obtain their electronic structure at a fraction of the complexity and computational effort required in a comparable all-electron calculation.

Specializing Eqs. (4) and (5) for atoms, the all-electron and pseudopotential single-particle equations are:

$$\left\{-\tfrac{1}{2}\nabla_r^2 - \frac{Z_c + Z_v}{r} + \frac{l(l+1)}{2r^2} + v_{ee}[\rho_c + \rho_v] + v_x[\rho_c + \rho_v] + v_{cr}[\rho_c + \rho_v]\right\}\psi_{nl}(r) = \varepsilon_{nl}\psi_{nl}(r) \tag{6}$$

and

$$\left\{-\tfrac{1}{2}\nabla_r^2 - \frac{Z_v}{r} + v_{ps}^{(l)}(r) + \frac{l(l+1)}{2r^2} + v_{ee}[n] + v_x[n] + v_{cr}[n]\right\}\chi_{nl}(r) = \lambda_{nl}\chi_{nl}(r) \tag{7}$$

respectively, where v_{ee}, v_x, and v_{cr} denote the density-functional interelectronic Coulomb, exchange, and correlation potentials and ∇_r is the radial Laplacien. In contrast to the empirical pseudopotential method (e.g., Cohen and Heine, 1970), $v_{ps}^{(l)}(r)$ in Eq. (7) is not determined by fitting the energies λ_{nl} to experiment, leaving the wavefunction χ_{nl} to be implicitly and arbitrarily fixed by such a process. Instead, we first construct physically desirable pseudo wavefunctions χ_{nl} and then solve for the pseudopotential $v_{ps}^{(l)}(r)$ that will produce these wavefunctions together with the theoretically correct orbital energies $\lambda_{nl} = \varepsilon_{nl}$ from the single-particle equation, Eq. (7).

To construct such pseudo wavefunctions, we postulate a number of constraints. We will first require that the pseudo wavefunction $\chi_{nl}(r)$ be given as a linear combination of the "true" all-electron core and valence orbitals of Eq. (6):

$$\chi_{nl}(r) = \sum_{n'} C_{n,n'}^{(l)} \psi_{n'l}^{c,v}(r) \tag{8}$$

Since the pseudo wavefunctions $\{\chi_{nl}(r)\}$ are now the lowest solutions to the pseudo-Hamiltonian, they will be nodeless for each of the lowest angular symmetries (e.g., while the all-electron 4s orbital of Cu has three nodes, the pseudo 4s orbital will have zero nodes, the 5s one node, etc.). The coefficients $\{C_{n,n'}^{(l)}\}$ will be, hence, chosen below to satisfy this condition. Note that in a single-determinental representation, such a mixing of rows and

columns leaves the energy invariant. We then require that the orbital energies λ_{nl} of the pseudopotential problem equal the "true" valence orbital energies ε_{nl}. The first constraint assures us that the pseudo wavefunctions are contained in the same core-plus-valence orbital space defined by the underlying density-functional theory; the second ensures that the spectral properties derived from the pseudopotential single-particle equation match those of the valence electrons in the all-electron problem.

Without specifying at this stage the choice of the unitary rotation coefficients $\{C^{(l)}_{n,n'}\}$, Eqs. (6)–(8) can already be solved to obtain the atomic pseudopotential $v^{(l)}_{ps}(r)$ in terms of the latter and the known quantities defining the all-electron atomic equation, Eq. (6):

$$v^{(l)}_{ps}(r)=\left\{U_l(r)-\frac{Z_v}{r}\right\}+\left\{-\frac{Z_c}{r}+v_{ee}[\rho_c]+v_x[\rho_c]+v_{cr}[\rho_c]\right\}$$
$$+\{v_x[\rho_c+\rho_v]-v_x[\rho_c]-v_x[\rho_v]\}+\{v_{cr}[\rho_c+\rho_v]-v_{cr}[\rho_c]-v_{cr}[\rho_v]\}$$
$$+\{v_{ee}[\rho_c]-v_{ee}[n]\}+\{v_x[\rho_v]-v_x[n]\}+\{v_{cr}[\rho_v]-v_{cr}[n]\} \quad (9)$$

where the "Pauli potential" $U_l(r)$ is given by

$$U_l(r)=\frac{\sum_{n'} C^{(l)}_{n,n'}[\varepsilon_{nl}-\varepsilon_{n'l}]\psi_{n'l}(r)}{\sum_{n'} C^{(l)}_{n,n'}\psi_{n,l}(r)} \quad (10)$$

and the core, valence, and pseudo charge densities are given as

$$\rho_c(r)=\sum_{nl}^{c}|\psi^c_{nl}(r)|^2$$
$$\rho_v(r)=\sum_{nl}^{v}|\psi^v_{nl}(r)|^2 \quad (11)$$
$$n(r)=\sum_{nl}^{v}|\chi_{nl}(r)|^2$$

One notices that in the pseudopotential representation each angular component of the system's wavefunction is experiencing a different external potential $v^{(l)}_{ps}(\mathbf{r})$, whereas in the regular, all-electron representation, $v_{ext}(\mathbf{r})$ was local [Eq. (4)]. This is a direct consequence of eliminating the subspace of core orbitals from explicit consideration, replacing thereby the dynamical effects of the core electrons by a static potential. Such a pseudopotential transformation allows us to conveniently decompose the chemically coded characteristics of the core into *orbital contributions.*

The atomic pseudopotential in Eq. (9) has a simple physical interpretation. The "Pauli potential" $U_l(r)$ is the only term in $v^{(l)}_{ps}(r)$ that depends on

the wavefunction it operates on (i.e, "nonlocal"), whereas all other terms in Eq. (9) are common to all angular momenta (i.e., "local"). Note that for atomic valence orbitals that lack a matching l-component in the core (e.g., carbon 2p or silicon 3d, lacking $l = 1$ and $l = 2$ core states, respectively), the all-electron valence orbital $\psi^{v}_{nl}(r)$ is nodeless—no mixing of other orbitals in Eq. (8) is needed for elimination of nodes. Hence, $\chi_{nl} = \psi_{nl}$ and, from Eq. (10), $U_l(r) = 0$ for such states. In these cases, the pseudopotential is local and purely attractive due to the dominance of the all-electron term, $-(Z_c + Z_v)/r$. In all other cases, $U_l(r)$ is positive and strongly repulsive, but confined to the atomic core region [for distances from the origin at which all core orbitals $\psi^{c}_{nl}(r)$ are small relative to the valence orbital $\psi^{v}_{nl}(r)$, the energy difference in the numerator causes $U_l(r)$ to be zero]. $U_l(r)$ replaces the core-valence orthogonality constraint and is a realization in coordinate space of Pauli's exclusion principle. Its precise form depends on the choice of the mixing coefficients $\{C^{(l)}_{n,n'}\}$ and is discussed below. We see that the pseudopotential nonlocality, often neglected in the empirical pseudopotential approach (Cohen and Heine, 1970; but compare Chelikowsky and Cohen, 1976; Pandey and Phillips, 1974) emerges naturally in this formulation from the quantum shell structure of the atom. Similarly, Phillips's pseudopotential kinetic energy cancellation theorem (e.g., Cohen and Heine, 1961) is simply represented as a cancellation (or over-cancellation) between the nonclassical repulsive Pauli potential and the core-valence Coulomb attraction $-Z_v/r$.

The second term in Eq. (9) represents the total screened potential set up by the core charge density $\rho_c(r)$. It approaches $-Z_c/r$ at small distances and decays to zero exponentially at the core radius (with a characteristic core screening length) due to rapid screening of the core point charge by the core electrons. The third and fourth terms in Eq. (9) represent the nonlinearity of the exchange and correlation potentials, respectively, with respect to the interference of ρ_c and ρ_v. They measure the core-valence interactions in the system and are proportional to the penetrability of the core by the valence electrons.

The fifth term in Eq. (9) is the Coulomb orthogonality hole potential. It has its origin in the charge fluctuation $\Delta(r) = \rho_v(r) - n(r)$ that results from the removal of the nodes in the pseudo wavefunctions [i.e., the transformation in Eq. (8)]. The electrostatic Poisson potential set up by $\Delta(r)$ is then given by the fifth term in Eq. (9). Finally, the last two terms in Eq. (9) represent, respectively, the exchange and correlation potentials set up by this orthogonality hole charge density $\Delta(r)$.

The form of the first-principles pseudopotential in Eqs. (9)–(10) makes it easy to establish contact with the successfully simplified early empirical pseudopotentials. Hence, for example, in the Abarenkov-Heine (1965) model

potential it was implicitly assumed that a pseudopotential cancellation between a repulsive Pauli force and an attractive Coulomb potential $-Z_v/r$ exists, but instead of calculating the spatial details of the cancellation its net result was assumed to take the form of a constant $v_{ps}^{(l)}(r) = A_l$ for r smaller than some radius R_l (i.e., inside the core), with $v_{ps}^{(l)}(r) = -Z_v/r$ for $r > R_l$. Abarenkov and Heine's empirical constants A_l may be identified in the present formulation with the volume integral of $[U_l(r) - Z_v/r]$ from the origin to R_l [neglecting all but the first term in Eq. (9)]. Similarly, Ashcroft (1966) has suggested an empirical "empty core" pseudopotential, postulating that the net result of the cancellation between $U_l(r)$ and $-Z_v/r$ inside the core region is zero. Indeed, for a sufficiently large core radius (i.e., of the order of Pauling's ionic radius), such a simple model represents well $v_{ps}^{(l)}(r)$ in Eq. (9).

Up to this point, we have not yet specified the form of the transformation coefficients in Eq. (8) determining the precise relationship between the pseudo and "true" wavefunctions. Clearly, one would like to constrain the pseudo wavefunction in Eq. (8) to be normalized. In addition, the relaxation of the orthogonality constraint may be exploited to construct $\chi_{nl}(r)$ as nodeless for each of the lowest angular states, permitting thereby a convenient expansion of the pseudo wavefunctions in spatially simple and smooth basis functions. Even so, $\chi_{nl}(r)$ is underdetermined: there are an infinite number of choices of $\{C_{n,n'}^{(l)}\}$ leading to normalized and nodeless $\chi_{nl}(r)$. This is a manifestation of the well-known pseudopotential nonuniqueness. The resolution of this nonuniqueness is precisely the point at which one applies one's physical intuition (and physical prejudices). Note, however, that in the present approach, any of the infinite and legitimate choices of $\{C_{n,n'}^{(l)}\}$ permits a rigorous digression from the pseudo wavefunction to the true valence wavefunction: the choice of a *linear* form for $\chi_j(r)$ in Eq. (8) allows for $v_{ps}^{(l)}(r)$ to be computed from an arbitrary set $\{C_{n,n'}^{(l)}\}$ and for the resulting pseudopotential to be used to greatly simplify the calculation of the electronic structure of arbitrary molecules or solids. Upon completion, one can simply recover the true wavefunction through a core orthogonalization:

$$\psi_j(\mathbf{r}) = \frac{1}{N}\{\chi_j(\mathbf{r}) - \sum_i^{\text{core}} \langle \chi_i | \psi_i^c \rangle \psi_i^c(r)\} \tag{12}$$

given the known core states $\psi_i^c(r)$. This property is not shared by other pseudopotentials (e.g., Kerker, 1980; Chelikowsky and Cohen, 1976). The choice of $\{C_{nn'}^{(l)}\}$ has, however, a direct bearing on the *transferability* of the atomic pseudopotentials from one system to another as well as on the degree to which the true valence wavefunctions can be reproduced without resort to core orthogonalization. Our choice of wavefunction transformation coefficients (Zunger, 1979) is based simply on *maximizing the similarity between the true and pseudo orbitals* [within the form of Eq. (8)] with a minimum core

amplitude, subject to the constraints that $\chi_{nl}(r)$ be normalized and nodeless. This simple choice produces highly energy-independent, and thus transferable, pseudopotentials, and at the same time the imposed wavefunction similarity leads to pseudo wavefunctions that retain the full chemical information contained in the valence region of the "true" wavefunctions. Details of the numerical procedure used to obtain $\{C^{(l)}_{n,n'}\}$ are given elsewhere (Zunger and Ratner, 1978; Zunger, 1979). The underlying principle for obtaining maximal wavefunction similarity can however be demonstrated with a simple example. Consider a first-row atom having a single 1s core state. The pseudo-orbitals according to Eq. (8) have the form:

$$\begin{aligned}\chi_{2s}(r) &= C^{(0)}_{1s,2s}\psi^{c}_{1s}(r) + C^{(0)}_{2s,2s}\psi^{v}_{2s}(r)\\ \chi_{2p}(r) &= \psi^{v}_{2p}(r)\end{aligned} \tag{13}$$

Normalization leads to:

$$[C^{(0)}_{1s,2s}]^2 + [C^{(0)}_{2s,2s}]^2 = 1 \tag{14}$$

Imagine now starting from $C^{(0)}_{1s,2s} = 0$ and $C^{(0)}_{2s,2s} = 1$ and gradually increasing $C^{(0)}_{1s,2s}$ from zero, keeping $C^{(0)}_{2s,2s} = (1 - C^2_{1s,2s})^{\frac{1}{2}}$. With more core character included, the node in $\psi^{v}_{2s}(r)$ shifts towards the origin. The first point at which the node coincides with the origin, giving a legitimately nodeless $\chi_{2s}(r)$, occurs at

$$\chi_{2s}(0) = 0 = C^{(0)}_{1s,2s}\psi^{c}_{1s}(0) + C^{(0)}_{2s,2s}\psi^{v}_{2s}(0) \tag{15}$$

Given the values of the all-electron orbitals ψ^{c}_{1s} and ψ^{v}_{2s} at the origin, Eqs. (14)–(15) determine, therefore, the expansion coefficients and hence the atomic pseudopotential in Eq. (9). One can imagine, however, a process in which one continues to mix core character over and beyond what is necessary just to eliminate the node in $\chi_{2s}(r)$. This continues to produce legitimate $\chi_{2s}(r)$ orbitals in the sense that they are nodeless. However, due to the admixture of excess ψ^{c}_{1s}, the similarity of χ_{2s} to the true ψ^{v}_{2s} decreases. Hence, the maximum similarity criterion becomes identical in this case with the condition that $\chi_{nl}(r = 0) = 0$, or a minimal core content in $\chi_{nl}(r)$. The vanishing value of $\chi_{nl}(r)$ at the origin causes the repulsive Pauli potential $U_l(r)$ in Eq. (10) to have a singularity at the origin since $v^{(l)}_{ps} \sim U_l(r) \sim \dfrac{\nabla^2_r \chi_l(r)}{\chi_l(r)}$. Combining such a positive and strongly repulsive $U_l(r)$ with the negative core attraction term $-Z_v/r$ in Eq. (9) leads necessarily to a hard-core-type pseudopotential with a characteristic crossing point $v^{(l)}_{ps}(r^0_l) = 0$ at $r = r^0_l$. *The occurrence of hard-core pseudopotentials with their attendant orbital radii r^0_l is therefore a consequence of the chemically motivated constraint that the pseudo wavefunctions of the form in Eq.* (8) *have the maximum possible similarity to the true valence*

wavefunction in the chemically important tail region. This short-range repulsive nature of $U_l(r)$ builds into the first-principles pseudopotentials the high momentum components absent in the empirical pseudopotentials (Cohen and Heine, 1970) that are fit to experimental energies alone.

In the more general case of an atom belonging to an arbitrary row in the periodic table, obtaining maximal wavefunction similarity is formulated as a constrained minimization of the core projection of the pseudo wavefunctions (e.g., Zunger, 1979). The general small-r expansion of the pseudo orbital becomes

$$\lim_{r\to 0} \chi_{nl}(r) = A_0 r^{\eta+1} + A_1 r^{\eta+1+1} + A_2 r^{\eta+1+2} \tag{16}$$

The choice of $\eta \geqslant 2$ leads to a minimum core amplitude pseudo wavefunction with its attendant maximum similarity to the true valence wavefunction. Inserting Eq. (16) into Eqs. (10) and (9) leads, for *any* $\eta \geqslant 2$, to:

$$\lim_{r\to 0} v_{ps}^{(l)}(r) = \frac{\tilde{B}_l}{r^2} - \frac{Z_v}{r} + \cdots \tag{17}$$

Hence, the Simons–Bloch (1973) empirical pseudopotential [Eq. (2)] is recovered as the small-r limit of the first-principles pseudopotential. Clearly, however, at finite r-values, the present potential [Eq. (9)] differs substantially from the Simons–Bloch form. The choice $\eta = 0$ leads to a soft-core pseudopotential [$\lim_{r\to 0} v_{ps}^{(l)}(r) = \text{constant}$]. The associated pseudo wavefunction is now finite at the origin, leading necessarily to a reduced similarity between the true and pseudo wavefunctions in the chemically relevant valence region. Our choice of the wavefunction transformation in Eq. (8) produces, therefore, unique pseudopotentials by going to the extreme limit of wavefunction similarity that is possible within the underlying density-functional orbital space.

Other possibilities for choosing pseudo wavefunctions exist and are discussed elsewhere (Zunger and Cohen, 1979b; Zunger, 1979; Redondo *et al.*, 1977). These procedures involve various ways of constructing pseudo wavefunctions from components lying *outside the density-functional orbital space* [unlike Eq. (8)] and do not maintain physically transparent analytical forms such as in Eqs. (9)–(10). Hence, to distinguish them from the present density-functional pseudopotentials, we refer to these as trans-density-functional (TDF) pseudopotentials. Although such procedures lead sometimes to a somewhat better numerical accuracy in the wavefunctions, we restrict ourselves in what follows to the conceptually simpler density-functional pseudopotentials.

The approach described above for constructing orbital-dependent pseudopotentials can easily be extended to spin- and orbital-dependent potentials

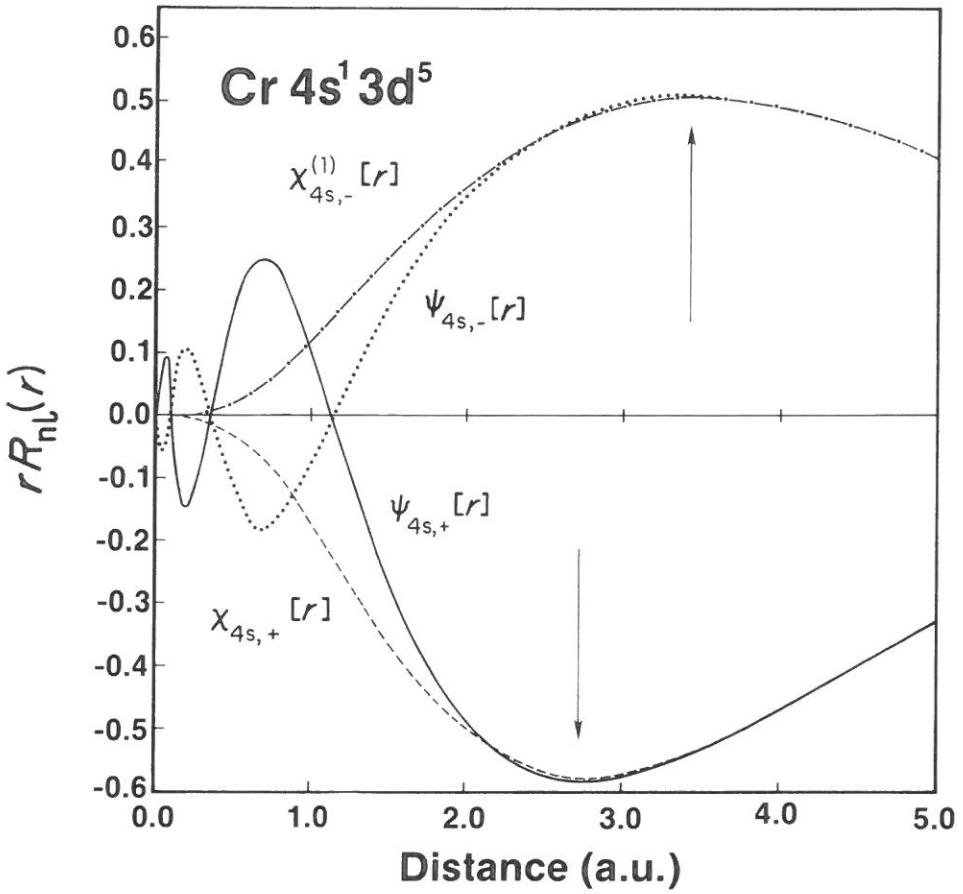

Fig. 1. Comparison of the 4s all-electron $[\psi_{4s\uparrow}(r), \psi_{4s\downarrow}(r)]$ and pseudo $[\chi_{4s\uparrow}(r), \chi_{4s\downarrow}(r)]$ wavefunctions of the Cr atom for spin up(↑) and down(↓).

(Zunger, 1980a). This generalization is simple, and we will not describe the details here, but rather give an illustrative example. Figure 1 compares the spin-up and spin-down pseudo wavefunction $\chi_{4s\uparrow}(r)$ and $\chi_{4s\downarrow}(r)$, which are eigenstates of the pseudo-Hamiltonian for the Cr atom, with the all-electron density-functional orbitals $\psi^{v}_{4s\uparrow}(r)$ and $\psi^{v}_{4s\downarrow}(r)$. The two sets of orbitals match very closely from $r = \infty$ up to a point $r \approx 2$ a.u., which lies inwards to the outer maximum of the true valence wavefunction. Hence, most bonding effects should be reasonably reproduced by the pseudo wavefunctions.

Figure 2 depicts various components of the $l = 0$ atomic pseudopotential in Eq. (9) for Sb. The curve labeled (1) is the Pauli term $U_1(r)$, the curve labeled (2) shows the $-Z_v/r$ term, and curve (3) represents all other terms in Eq. (9). Finally, curve (4) shows the total pseudopotential. Figure 3 shows the atomic pseudopotential for the second-row atoms, and Fig. 4 shows similar results for the transition elements. First-principles atomic pseudopotentials were generated for 70 atoms with $2 \leqslant Z \leqslant 57$ and $72 \leqslant Z \leqslant 86$ (i.e., the first five rows).

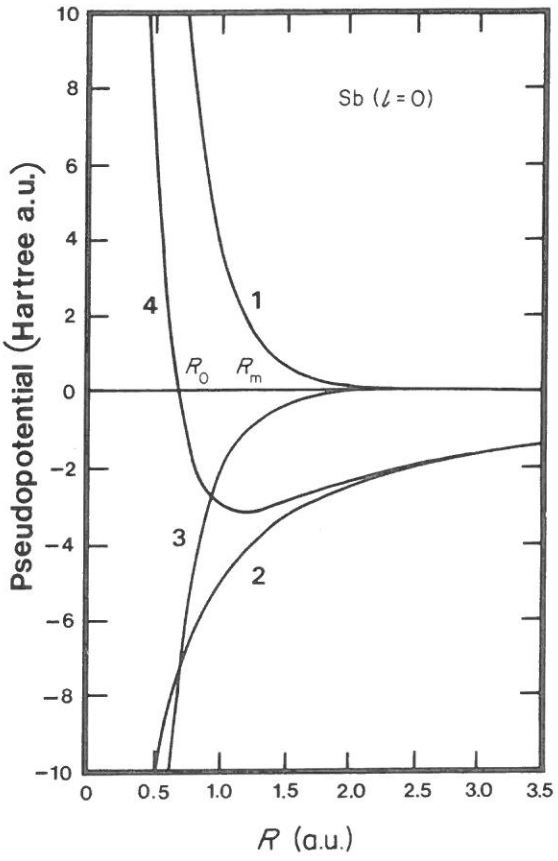

Fig. 2. Components of the atomic pseudopotential $v_{ps}^{(1)}(r)$ [Eq. (9)] for $l = 0$ of the Sb atom: (1) Pauli potential $U_1(r)$; (3) core screening; (2) the Coulomb attraction $-Z_v/r$; and (4) the total pseudopotential. R_0 and R_m denote the points of crossing and minimum, respectively.

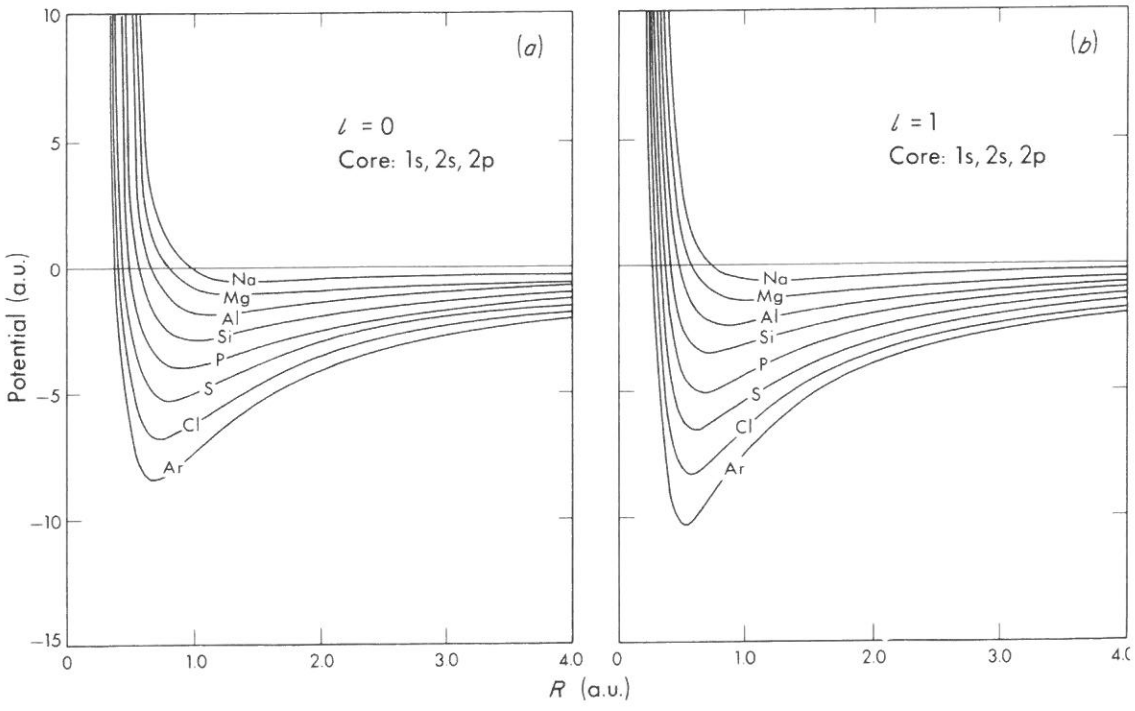

Fig. 3. Atomic pseudopotentials for the second-row atoms: (*a*) s potentials; (*b*) p potentials [Eq. (9)].

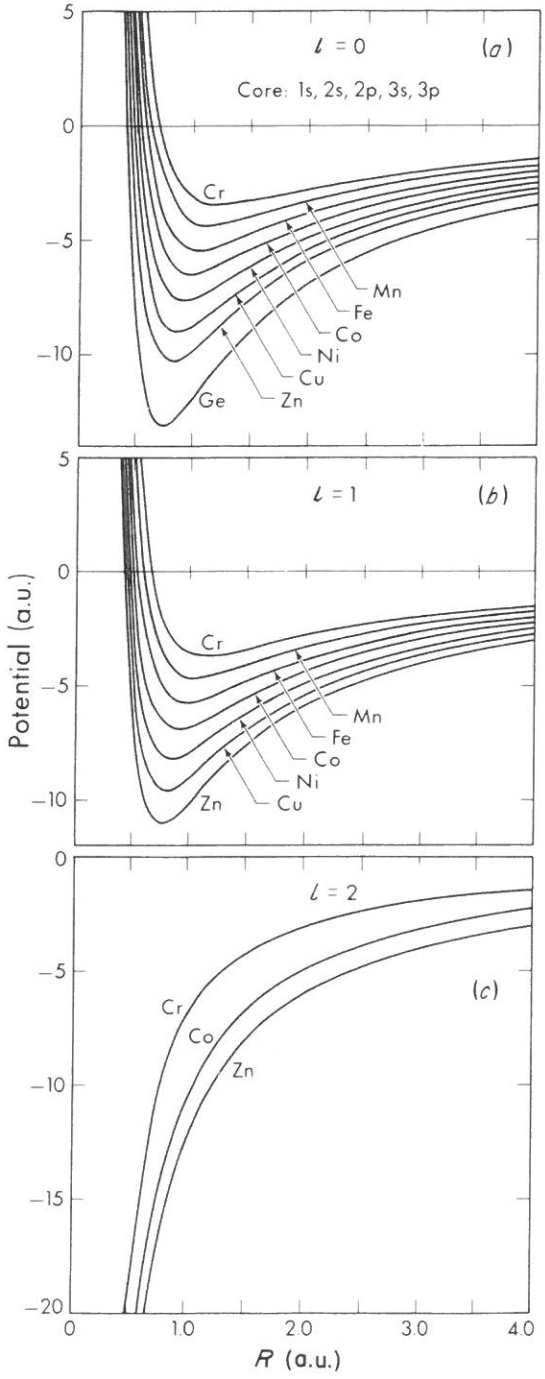

Fig. 4. Atomic pseudopotentials for the 3d elements: (*a*) s potentials; (*b*) p potentials; (*c*) d potentials [Eq. (9)]. Note that due to the absence of core states of $l = 2$ symmetry, the d potential for this row is purely attractive.

A notable feature of these "hard-core" potentials is the occurrence of a crossing point $v_{ps}^{(l)}(r_l^0) = 0$ at $r = r_l^0$. From Eqs. (9)–(10), it is seen that, physically, this point is where the repulsive Pauli potential is balanced by the Coulomb attraction $-Z_v/r$, renormalized by the screened core potential, exchange-correlation nonlinearity, and the Coulomb and exchange-correlation orthogonality hole potentials.

It seems somewhat puzzling at first sight that pseudopotentials of free-electron-like metals such as Na, Al, and K may have large momentum components or even a hard core, because the nearly-free-electron (NFE) model seems to have worked so well for these materials. However, the successes of the NFE model may have been overstated, in view of the fact that *wavefunction-related properties* of the free-electron metals, such as the shape of the optical conductivity (Bennett and Vosko, 1972), the metallic ground-state charge density and form-factors (Walter *et al.*, 1973; compare, however, with Bertoni *et al.*, 1973; Hafner, 1978), as well as the properties of impurities in metals (Hodges, 1977), are poorly reproduced by local and weak pseudopotentials. Moreover, the occurrence of rather complex crystal structures involving "simple" free-electron atoms (semimetals such as the B32 structure of LiAl, Laves phase materials such as K_2Cs, the existence of the compound Na_2K but not NaK or NaK_7, etc.) as well as the existence of stable multiple valencies of these systems (e.g., AlF vs. AlF_3, etc.) cannot be understood in terms of local NFE pseudopotentials. Hence, although such weak and NFE pseudopotentials had to be assumed for many elements (including Groups IIIA–VIA atoms) for the very popular low-order perturbation theories to be valid, the underlying assumption—that the complex chemistry of the related compounds could be understood in terms of weak and isotropic perturbations of a homogeneous electron gas—seems naive. However, the great analytical beauty of the perturbation theory approaches (Harrison, 1966) need not be sacrificed when hard-core pseudopotentials are used. Instead, a new definition is necessary for the unperturbed system as a suitably *nonhomogeneous* form, including most of the chemically relevant potential fluctuations in zero order (Simons–Bloch pseudopotentials? square wells?).

Using the calculated atomic pseudopotentials of Eqs. (9)–(11), we now define the crossing points using the ground-state *screened* atomic pseudopotentials $v_{\mathrm{eff}}^{(l)}(r)$:

$$v_{\mathrm{eff}}^{(l)}(r) = v_{\mathrm{ps}}^{(l)}(r) + \frac{l(l+1)}{2r^2} + v_{\mathrm{ee}}[n] + v_{\mathrm{x}}[n] + v_{\mathrm{cr}}[n] \tag{18}$$

as:

$$v_{\mathrm{eff}}^{(l)}(r_l) = 0$$

Here $v_{\mathrm{eff}}^{(l)}(r)$ is the total effective potential experienced in a ground-state pseudo atom by electrons with angular momentum l. These form the structural indices $\{r_l\}$, which we use in connection with predicting the stable crystal structure of compounds. Table I gives the $\{r_l\}$ values of the 70 elements

TABLE I

Classical Crossing Points of the Self-Consistently Screened Nonlocal Atomic Pseudopotentials (Including the Centrifugal term) (a.u.)[a]

Atom	r_s	r_p	r_d	Atom	r_s	r_p	r_d
Li	0.985	0.625	—	Rb	1.67	2.43	0.71
Be	0.64	0.44	—	Sr	1.42	1.79	0.633
B	0.48	0.315	—	Y	1.32	1.62	0.58
C	0.39	0.25	—	Zr	1.265	1.56	0.54
N	0.33	0.21	—	Nb	1.23	1.53	0.51
O	0.285	0.18	—	Mo	1.22	1.50	0.49
F	0.25	0.155	—	Tc	1.16	1.49	0.455
Ne	0.22	0.14		Ru	1.145	1.46	0.45
				Rh	1.11	1.41	0.42
Na	1.10	1.55		Pd	1.08	1.37	0.40
Mg	0.90	1.13	—	Ag	1.045	1.33	0.385
Al	0.77	0.905	—	Cd	0.985	1.23	0.37
Si	0.68	0.74	—	In	0.94	1.11	0.36
P	0.60	0.64	—	Sn	0.88	1.00	0.345
S	0.54	0.56	—	Sb	0.83	0.935	0.335
Cl	0.50	0.51	—	Te	0.79	0.88	0.325
Ar	0.46	0.46	—	I	0.755	0.83	0.315
				Xe	0.75	0.81	0.305
K	1.54	2.15	0.37				
Ca	1.32	1.68	0.34	Cs	1.71	2.60	
Sc	1.22	1.53	0.31	Ba	1.515	1.887	0.94
Ti	1.15	1.43	0.28	La	1.375	1.705	0.874
V	1.09	1.34	0.26	Hf	1.30	1.61	0.63
Cr	1.07	1.37	0.25	Ta	1.25	1.54	0.605
Mn	0.99	1.23	0.23	W	1.22	1.515	0.59
Fe	0.95	1.16	0.22	Re	1.19	1.49	0.565
Co	0.92	1.10	0.21	Os	1.17	1.48	0.543
Ni	0.96	1.22	0.195	Ir	1.16	1.468	0.526
Cu	0.88	1.16	0.185	Pt	1.24	1.46	0.51
Zn	0.82	1.06	0.175	Au	1.21	1.45	0.488
Ga	0.76	0.935	0.17	Hg	1.07	1.34	0.475
Ge	0.72	0.84	0.16	Tl	1.015	1.22	0.463
As	0.67	0.745	0.155	Pb	0.96	1.13	0.45
Se	0.615	0.67	0.15	Bi	0.92	1.077	0.438
Br	0.58	0.62	0.143	Po	0.88	1.02	0.425
Kr	0.56	0.60	0.138	At	0.85	0.98	0.475
				Rn	0.84	0.94	0.405

[a] The core shell is defined in each case as the rare-gas configuration of the preceding row. The Kohn and Sham exchange is used.

for which the density-functional pseudopotential equations have been solved. We have not included the heavier elements since the present pseudopotential theory is nonrelativistic. In what follows, we will hence not discuss the structural stability of lanthanide and actinide compounds.

The structure of Eq. (18) reflects our discussion in the Introduction concerning the quantum-mechanical and semiclassical viewpoints of electronic structure: $v_{ps}^{(l)}(r)$ is the realization of the quantum-mechanical electron-core potential $V_{ec}(\mathbf{r}, \mathbf{R})$, whereas the last three terms in Eq. (18) represent the interelectronic potential $V_{ee}(\mathbf{r}, \mathbf{r}')$. The semiclassical factors are then represented by the $\{r_l\}$ scale implicit in the screened effective potential.

In developing the density-functional pseudopotentials, we have tacitly assumed a specific partitioning of the atomic orbitals into core and valence. In the present theory, core orbitals are those appearing as closed-shell states in the rare gas atom of the preceding row in the periodic table. Note, however, that although we may understand the low-energy electronic excitation spectra of a compound such as ZnSe by assuming that the Zn 3d orbitals belong to in a passive core state, such an assumption may be invalid in intermetallic compounds, where the Zn 3d orbitals can be in near resonance with the d orbitals of another element (e.g., CuZn). Given the fact that any such delineation into core and valence is merely based on an arbitrary assumption on the passivity of certain selected orbitals to chemical perturbations of interest, one may ask whether structurally meaningful orbital radii can be extracted from a pseudopotential scheme.

In fact, the choice of the orbital radii from the *screened* pseudopotential [Eq. (18)], rather than from the *bare* pseudopotential $v_{ps}^{(l)}(r)$ in Eq. (9) (e.g., Simons and Bloch, 1973; Andreoni *et al.*, 1979), is based precisely on an attempt to avoid such a nonuniqueness. Although the bare pseudopotential of Eq. (9) has the form

$$v_{ps}^{(l)}(r) = U_l(r) + f(Z_c, Z_v, \rho_c, \rho_v, n) \tag{19}$$

the *screened* pseudopotential can be written as

$$V_{eff}^{(l)}(r) = U_l(r) + g(Z, \rho_c + \rho_v) \tag{20}$$

Note that whereas $U_l(r)$ [Eq. (10)] depends only on orbitals with angular momentum l, the valence pseudo charge density $n(r)$ [Eq. (11)] depends on all orbitals that are assigned as valence states. Consequently, if the Zn 3d orbitals are assumed to belong to the core, the *bare pseudopotential* $v_{ps}^{(l)}(r)$ for s and p electrons is different than if the d electrons were assigned to the valence. In contrast, it follows from Eq. (20) that the *screened pseudopotential* $v_{eff}^{(l)}(r)$ for $l = 0, 1$ is invariant under such a change in the assignment of the d electrons. Our definition of the structural indices r_l is therefore independent of the assignment of orbitals $\psi_{nl}(r)$ from other angular shells as

core or valence. Also note that the definition of orbital radii from the screened pseudopotentials of Eq. (18) permits a direct inclusion of electronic exchange and correlation effects in the structural coordinates r_l (see Schubert, 1977), whereas the semiclassical electron concentration factor (Hume-Rothery and Raynor, 1954) is represented simply by Z_v.

B. Simple Universal Form of the Density-Functional Pseudopotential

The idea of atomic radii is not new in pseudopotential theory (see Sec. II). The basic thrust of the pseudopotential concept is to transform the chemical picture of the existence of an *orbital subspace* of nearly chemically inert core states into a delineation either in *configuration space* or in *momentum space* of a core region of the potential (with its attendant cancellation effects between orthogonality repulsion and Coulomb attraction) and a valence region (with its weaker effective potential). What is new in our present approach is that whereas in the empirical pseudopotential methods the radii were imposed *extraneously*, either explicitly (Abarenkov and Heine, 1965; Ashcroft, 1966; Shaw, 1968; Simons and Bloch, 1973; Natapoff, 1975, 1976, 1978) or implicitly (Cohen and Bergstresser, 1966), the present theory provides them as a natural fingerprint of the internal quantum structure of the isolated atom. Hence, although the empirical pseudopotential methods assumes the existence of opposing forces in the core region leading to the occurrence of a delineating radius, in these approaches the forces are not calculated. The radii are in turn transferred from various sources (Pauling ionic radii, the position of the last node in the valence s orbital, fitting energy eigenvalues to atomic term values, optical reflectivity of semiconductors, or the Fermi surface of metals, etc.), such that although a desired fit to selected experimental observables is achieved, the underlying electronic and structural regularities may be obscured by fitting to different data or by postulating certain arbitrary analytic forms for $v_{ps}^{(l)}(r)$.

Given that the analytic form of the pseudopotential in the present approach is not assumed but rather emerges as a consequence of requiring a maximum similarity between the all-electron and pseudo wavefunctions in the chemically important tail region, it however is possible to deduce a posteriori a universal analytic form. The density-functional atomic pseudopotentials have been calculated numerically from Eqs. (9)–(11), given the all-electron density-functional wavefunctions and orbital energies (Zunger and Cohen, 1978b). In the present study, we use the orbital radii $\{r_l\}$ determined from Eq. (18) (Table I) and these numerical pseudopotentials. However, because the limiting behavior of all terms entering the pseudopotentials in Eqs. (9)–(10) is known, one can obtain an *approximate explicit analytical form* for these

pseudopotentials through fitting to the numerical results. Such a fit can be done in two different ways: either emphasizing a high numerical accuracy for the fit (and hence using rather complicated fitting functions) or by using a physically transparent fitting function, sacrificing to some extent the numerical accuracy but obtaining the correct *regularities* of the pseudopotentials. This has been attempted by Lam *et al.* (1980) using the simple form:

$$v_{ps}^{(l)}(r) \approx \frac{C_{1l}}{r^2} e^{-C_{2l}r} - \frac{Z_c}{r} e^{-C_3 r} - \frac{Z_v}{r} \tag{21}$$

The coefficients $\{C_{1l}, C_{2l}, \text{and } C_3\}$ are tabulated by Lam *et al.* Although more complicated forms than Eq. (21) have also been used (Lam *et al.*, 1980), Eq. (21) reveals a very important characteristic of the density-functional pseudopotentials: to within a reasonable approximation, the constants C_{1l}, C_{2l}, and C_3 are *linear* functions of the atomic number, i.e.,

$$C_{1l} \approx a_l + b_l Z; \qquad C_{2l} \approx c_l + d_l Z; \qquad C_3 \approx e + fZ \tag{22}$$

This constitutes a significant reduction in the number of degrees of freedom required to specify the potential and reveals the regularities of the periodic table through the coordinates (Z_c, Z_v). This can be contrasted with the empirical pseudopotential approach in which such regularities are often obscured by fitting certain atomic pseudopotentials to optical data (Cohen and Bergstresser, 1966), whereas others are fit to metallic Fermi-surface data and the resistivity of metals (Ashcroft, 1966, 1968; Ashcroft and Langreth, 1967) or to atomic term values (Szasz and McGinn, 1967; Simons, 1971a,b; Abarenkov and Heine, 1965).

The existence of a simple linear scaling relationship in Eqs. (21)–(22) establishes a mapping of Mendeleyev's classical dual coordinates Z_c and Z_v characterizing the digital structure of the periodic table, into a more refined quantum-mechanical coordinate system, $r_s(Z_c, Z_v)$, $r_p(Z_c, Z_v)$, and $r_d(Z_c, Z_v)$. Given the fact that Mendeleyev's dual coordinates (Z_c, Z_v) are already suggestive of broad structural trends (e.g., the AB compounds with $Z_v^A = 3$ and $Z_v^B = 5$ tend to form zinc blende structures for large $Z_c^{A,B}$ values, while compounds with $Z_v^A = 1$ and $Z_v^B = 7$ tend to form rock-salt structures, etc.), it is only reasonable to expect that with their present resolution into anisotropic orbital components, far more sensitive structural coordinates can be achieved.

C. Application to Electronic Structure Calculations

As discussed in Sec. II, properly constructed pseudopotentials can be used for self-consistent electronic structure calculations for molecules and solids

in a way that is much simpler than the all-electron approach—or for using the periodic chemical regularities coded in the pseudopotentials to abstract structurally significant semiclassical-like scales. In this section, we briefly summarize the first application; in the following section (IV), we discuss the structural significance of the pseudopotentials.

In using pseudopotentials for electronic structure calculations, one constructs the solid-state pseudopotential $V_{ps}^{(l)}(\mathbf{r})$ as a superposition of the transferable *atomic* pseudopotentials $v_{ps}^{(l)}(r)$. The screening $V_{scr}[n(\mathbf{r})]$ is then calculated from the self-consistent response of the valence electrons in the *solid* to this external potential. Before describing applications to electronic structure, we wish to caution the reader in relation to two fundamental limitations of first-principles pseudopotentials. First, although any pseudopotential simplifies the description of many-electron systems by projecting out the often chemically passive core wavefunctions, its application is inherently limited to physical quantities that are largely unaffected by such core states. Hence, quantities such as the Fermi contact interactions, core spin polarization, Mössbauer core shifts, or core photoelectron spectra are entirely outside the realm of application of pseudopotential theories. Second, any first-principles pseudopotential theory, attempting to replace a given all-electron representation of the electronic structure, can give results that are no more refined than the physical assumptions underlying the all-electron theory it replaces. Hence, while empirical pseudopotentials attempt to directly mimic certain experimental observables through a parametrized fit, Hartree–Fock pseudopotentials (e.g., Kahn *et al.*, 1976) or the present density-functional pseudopotentials can produce results that are at best as accurate as is the respective all-electron theory. On the other hand, not only can the first-principles pseudopotentials be progressively refined as our understanding of many-electron correlation effects improves (e.g., Zunger *et al.*, 1980, also unpublished results; Zunger, 1980a), but, even more importantly, in the present approach both the successes and the failures of the theory in explaining experiment can be analyzed and understood in terms of well-defined quantum-mechanical constructs.

As an initial step in using atomic pseudopotentials, one has to establish exactly how transferable they are from one system to another. One way of testing this is to use the *atomically derived* pseudopotential to calculate a self-consistent pseudopotential band structure of a *solid* and compare the results with an all-electron band structure calculation in which no pseudopotentials are used. Such a comparison is given in Table II (D. R. Hamann, unpublished results, 1979), which shows data for crystalline silicon obtained with the TDF pseudopotential (Zunger and Cohen, 1979b; Zunger, 1979). It is seen that the pseudopotential calculation, considering only four valence

TABLE II

Comparison of the Band Structure of Crystalline Silicon as Obtained from an All-Electron (Core + Valence) Calculation and a Valence-Only Pseudopotential Calculation (eV)[a]

Level	All-electron	Pseudopotential	Level	All-electron	Pseudopotential
$\Gamma_{1,v}$	−12.02	−11.88	$X_{1,c}$	0.55	0.62
$\Gamma_{25,v}$	0.00	0.00	$X_{4,c}$	10.32	10.26
$\Gamma_{15,c}$	2.49	2.53	$L_{2',v}$	−9.64	−9.55
$\Gamma_{2',c}$	3.18	3.07	$L_{1,v}$	−7.06	−6.97
$\Gamma_{1,c}$	7.46	7.53	$L_{3,c}$	−1.16	−1.14
$\Gamma_{12,c}$	7.86	7.85	$L_{1,c}$	1.40	1.39
$X_{1,v}$	−7.84	−7.76	$L_{3,c}$	3.37	3.40
$X_{4,v}$	−2.82	−2.78			

[a] Using the TDF pseudopotential of Zunger (1979) and Zunger and Cohen (1979b). Results are obtained by a self-consistent linear-augmented-plane-wave method (D. R. Hamann, unpublished results, 1979) using the Wigner exchange and correlation potential.

electrons per Si atom, and the all-electron calculations, which include the full 14 electrons per Si atom, match within an average deviation of 0.06 eV over an energy range of valence and conduction bands of 20 eV. Another way of testing the pseudopotential energy dependence involves using an atomic pseudopotential derived from the *ground electronic configuration* in atomic self-consistent calculations for *excited configurations*. By means of exciting the atom (or ionizing a few electrons), a very wide range of wavefunction localization and orbital energies can be probed. This can be used to test whether the pseudopotential results continue to mimic the all-electron results away from the ground-state electronic configuration used to construct the pseudopotential. Extensive work (Zunger and Cohen, 1978b; Zunger, 1979) on many atoms indicates that the typical errors involved in orbital energies, total energy differences (i.e., excitation energies), and wavefunction moments are within 10^{-2}–10^{-4} eV, 10^{-3}–10^{-4} eV, and 0.1%–2%, respectively, over a range of about 20 eV of excitation energies. This satisfies our initial constraint that atomic pseudopotentials be constructed in a way that is approximately independent of their chemical environment.

The first-principles atomic pseudopotentials have been applied to self-consistent electronic structure calculations of polyatomic systems such as diatomic molecules—O_2 and Si_2 (Kerker *et al.*, 1979; Schlüter *et al.*, 1979); tetrahedrally bonded semiconductors—silicon (D. R. Hamann, unpublished results, 1979; Zunger and Cohen, 1979b), Ge (Zunger and Cohen, 1979b), and GaAs (Zunger, 1980b); as well as elemental transition-metal solids—Mo and W (Zunger *et al.*, 1979a; Zunger and Cohen, 1979a). In addition, these

TABLE III

Calculated and Observed Equilibrium Lattice Constant a_{eq} (Å), Total Valence Energy E_t (Rydberg), or Cohesive Energy ΔE_0 (eV), and Bulk Modulus B (dyn/cm^2) for Crystalline Silicon, bcc Tungsten, and Molybdenum[a]

		a_{eq}	E_t or ΔE_0	B (10^{12} dyn/cm^2)
Si	Observed	5.43	−7.919[b]	0.99
	Calculated	5.44	−7.959[b]	0.94
Mo	Observed	3.147	6.82[c]	3.23
	Calculated	3.15	6.68[c]	3.45
W	Observed	3.165	8.90[c]	2.73
	Calculated	3.17	7.90[c]	3.05

[a] Calculated results are obtained using the first-principles atomic pseudopotentials and a self-consistent mixed-basis approach (Zunger, 1980c; Zunger and Cohen, 1979a).

[b] Total valence energy (Ryd).

[c] Cohesive energy (eV).

pseudopotentials were used in the first nonlocal calculations dealing with a semiconductor surface—GaAs (110) (Zunger, 1980b), transition-metal impurities in crystalline silicon (U. Lindefelt and A. Zunger, unpublished, 1981), and the Ge–GaAs semiconductor interface (A. Zunger, unpublished results, 1980). The scope of this article does not warrant the description of detailed results, and the interested reader is referred to the original papers. Here, we will give two examples illustrating the level of agreement between these calculations and experiment.

Table III shows the predicted and observed equilibrium lattice constant a_{eq}, bulk modulus B, and cohesive energy ΔE_0 (or total valence energy) for Mo, W, and Si in their observed stable crystal structure. These are obtained by solving the Schrödinger equation self-consistently with the effective potential of Eq. (5) and calculating the variational ground-state total energy using a mixed basis set of Gaussian orbitals and plane waves. The second example is given in Fig. 5, where the calculated pseudopotential charge density of bulk Si (Zunger, 1980c) is compared with the experimental bonding charge density (Yang and Coppens, 1974). Keeping in mind that no empirical input other than the crystal structure and the atomic number is used in all of these calculations, the level of agreement with experiment is striking. What has been demonstrated here is that the first-principles pseudopotential method is capable of producing transferable atomic potentials that in quantitative electronic structure calculations yield a chemical type of accuracy.

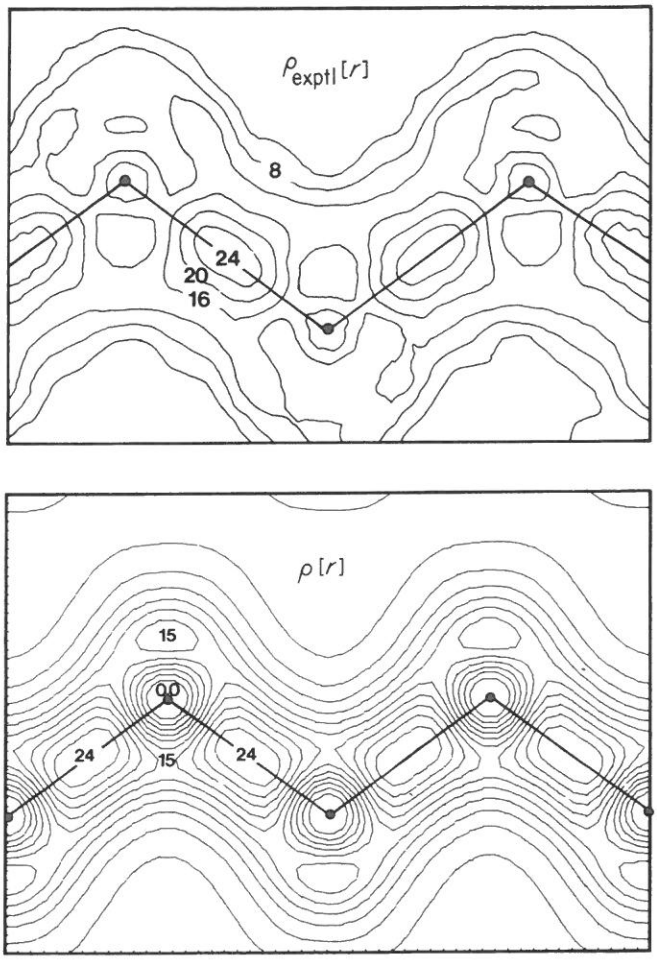

Fig. 5. Experimental [$\rho_{\text{exptl}}(\mathbf{r})$, Yang and Coppens (1974)] and calculated valence charge density of silicon in the (110) plane, in units of electron per cell. The calculation is based on the first-principles pseudopotential using a self-consistent mixed-basis method. Full dots indicate atomic positions.

IV. TRENDS IN ORBITAL RADII

A. Chemical Regularities

We have argued that the classical turning points r_l of the screened density-functional *atomic* pseudopotentials form a useful elemental distance scale for *solids*. One may then ask if indeed such atomic quantities retain their significance in the solid state. To answer this, we have performed a self-consistent band-structure calculation for bcc tungsten using our atomic pseudopotentials. This is done by assuming that the crystalline pseudopotential $V_{\text{ps}}^{(l)}(\mathbf{r})$ is a superposition of the atomic pseudopotentials $v_{\text{ps}}^{(l)}(r)$; but the screening $V_{\text{scr}}^{\text{v}}[n]$ is calculated from the self-consistent Bloch wavefunctions of the solid (Zunger

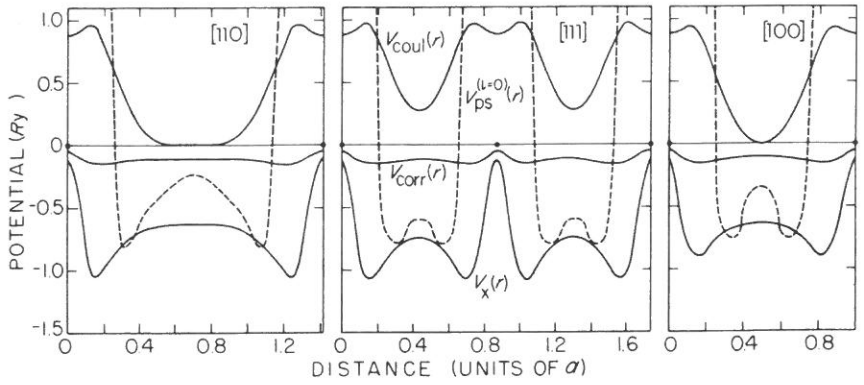

Fig. 6. The self-consistent screening potential [interelectronic Coulomb $V_{coul}(\mathbf{r})$, exchange $V_x(\mathbf{r})$, and correlation $V_{corr}(\mathbf{r})$] and pseudopotential $V_{ps}^{(l=0)}(\mathbf{r})$ for bcc tungsten in different directions in the crystal.

and Cohen, 1979a), rather than from atomic orbitals. The resulting band-structure, Fermi-surface, and optical spectra are in very good agreement with previously published experimental data. One can now use the self-consistent crystalline charge density $n(\mathbf{r})$, calculate the Coulomb, exchange, and correlation screening in the solid, and extract from that the screened solid-state pseudopotentials $V_{\text{eff}}^{(1)}(\mathbf{r})$ [Eq. (1)] their classical turning points. Obviously, such a solid-state screened potential has a different form in the different crystalline directions $[h, k, l]$, resulting in spatially anisotropic orbital radii $r_1[h, k, l]$. Figure 6 shows the solid-state tungsten pseudopotential (dashed lines) as well as the three components of the screening (evaluated with respect to the Fermi energy) in the solid. Although the screened pseudopotentials show a pronounced directional character, *the solid-state radii, lying in the core region of the atoms, show only a small anisotropy*: $r_0[111] = 1.279 \pm 0.002$ a.u., $r_0[001] = 1.214 \pm 0.002$ a.u., and $r_0[110] = 1.256 \pm 0.002$ a.u., compared with the isotropic atomic value $r_0 = 1.225$ a.u. and the average crystalline value of 1.25 a.u. The near invariance of these radii with respect to the chemical environment should be contrasted with the pronounced dependence of the classical crystallographic radii (e.g., Shannon and Prewitt, 1969) on chemical factors.

Inspection of the atomic pseudopotentials depicted in Figs. 3 and 4 immediately reveals clear regularities. This may be appreciated from Fig. 7, which shows the radius $r_1^{\min}$ at which the $l = 0$ pseudopotential has its minimum, plotted against the depth of the minimum W_1. The column structure of the periodic table is immediately apparent. At the upper left corner of the figure, we see elements such as Cs and Rb, characterized by a very shallow and extended pseudopotential; these elements are indeed the least electronegative in the first five rows of the periodic table. In the lower right corner, we find

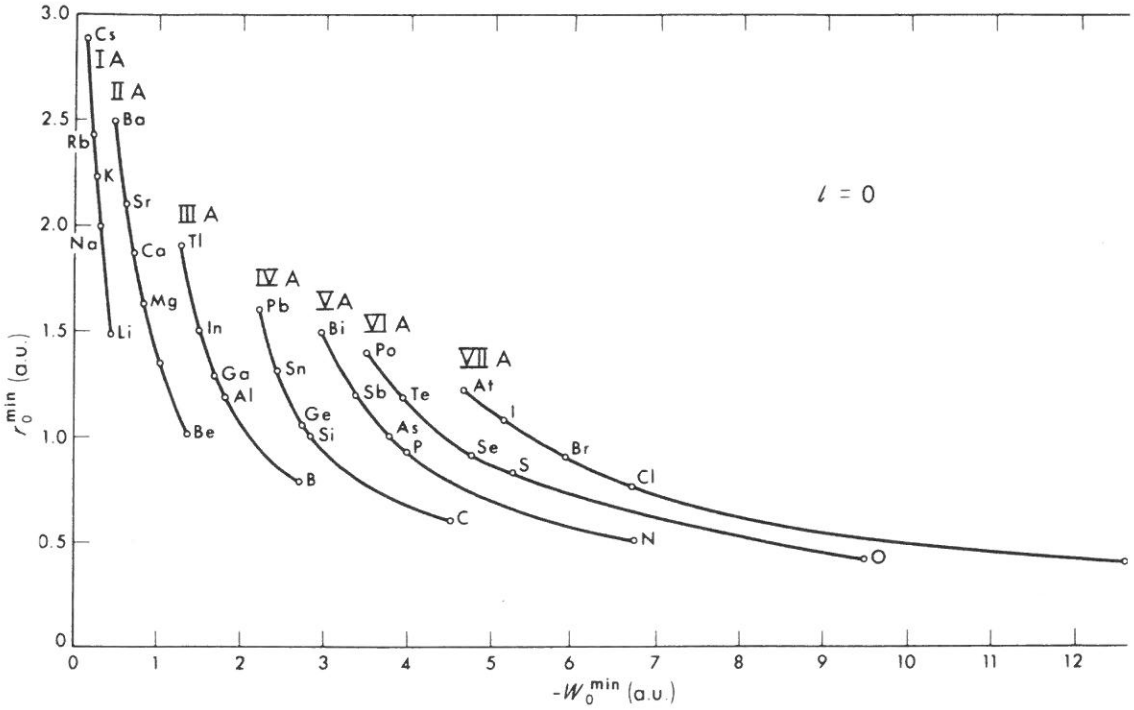

Fig. 7. The correlation between the radius r_0^{min} at which the s pseudopotential has its minimum and the depth of the minimum $-W_0^{min}$, for the nontransition elements.

elements such as F and O, which are characterized by very deep and localized pseudopotentials; these are indeed the most electronegative elements. Clearly, as the electronegativity is a measure of the power of an atom to gain extra electrons from its environment and at the same time keep its own electrons, such a propensity is reflected in the potential-well structure of $v_{ps}^{(l)}(r)$. In contrast with the thermochemical or dielectric electronegativity scales, however, the present orbital radii define an *anisotropic* (or *l*-dependent) electronegativity scale.

We see in Fig. 7 that the first-row elements are somewhat separated from the other elements—the former having deeper potentials than might have been expected from extrapolating the data for other rows. This phenomenon, resulting from a weak pseudopotential kinetic energy cancellation for the first-row elements, is also clearly reflected in the thermochemistry of the corresponding compounds. As we move from the right to the left of the periodic table, one sees in Fig. 7 that the elements belonging to a given column can be characterized solely by their potential radii, the potential depth being nearly constant. This seems to be the basis for the success of the "empty core" pseudopotentials (Ashcroft, 1966) postulated for simple metals, in which $v_{ps}(r)$ is assumed to be zero within a sphere of radius R_{ec}. Only the variation of R_{ec} within a column in the periodic table is used to characterize a large

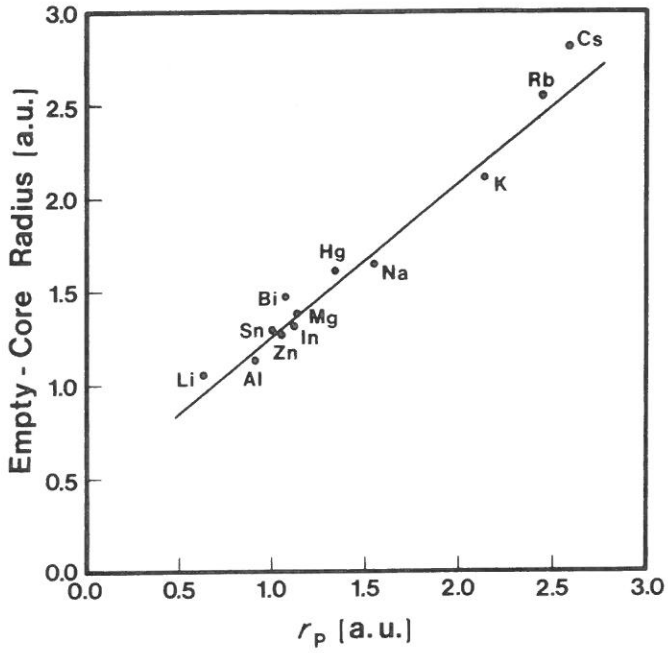

Fig. 8. Correlation between Ashcroft's empty-core pseudopotential radius and the p orbital radius of the present density-functional screened pseudopotential (Table I).

variety of transport and structural data for the corresponding metals (e.g., Ashcroft, 1966, 1968; Ashcroft and Langreth, 1967; Stroud and Ashcroft, 1971). In fact, one finds that these empirical empty core radii used to fit resistivity data may be identified, within a linear scale factor, with our r_p screened pseudopotential coordinate (Fig. 8). Whereas the alkali elements are characterized predominantly by a single coordinate (Fig. 7), in line with their free-electron properties associated with a shallow pseudopotential, the elements to their left are characterized by a dual coordinate system. The regularities in these dual coordinates also reflect well-known chemical trends: for example, the tendency towards metalization in the C, Si, Ge, Sn, and Pb series is represented by the increased delocalization and reduced depth in their pseudopotentials, etc.

To illustrate the significance of the angular momentum dependence of the atomic pseudopotentials, Fig. 9 shows the elements ordered by their $(r_l^{\min}, W_l)$ coordinates. The elements are clearly grouped according to their rows in the periodic table. At small $|W_l|$ and large $r_l^{\min}$ (i.e., shallow and delocalized, or weak, potentials), we find the classical free-electron-like metals; at large $|W_l|$ and small $r_l^{\min}$ (deep and localized, or strong, potentials) we find the atoms that form covalent structures and the transition elements. Each row in the periodic table is represented here by at least two lines—one connecting the full circles passing through the $l = 0$ coordinates and one connecting open

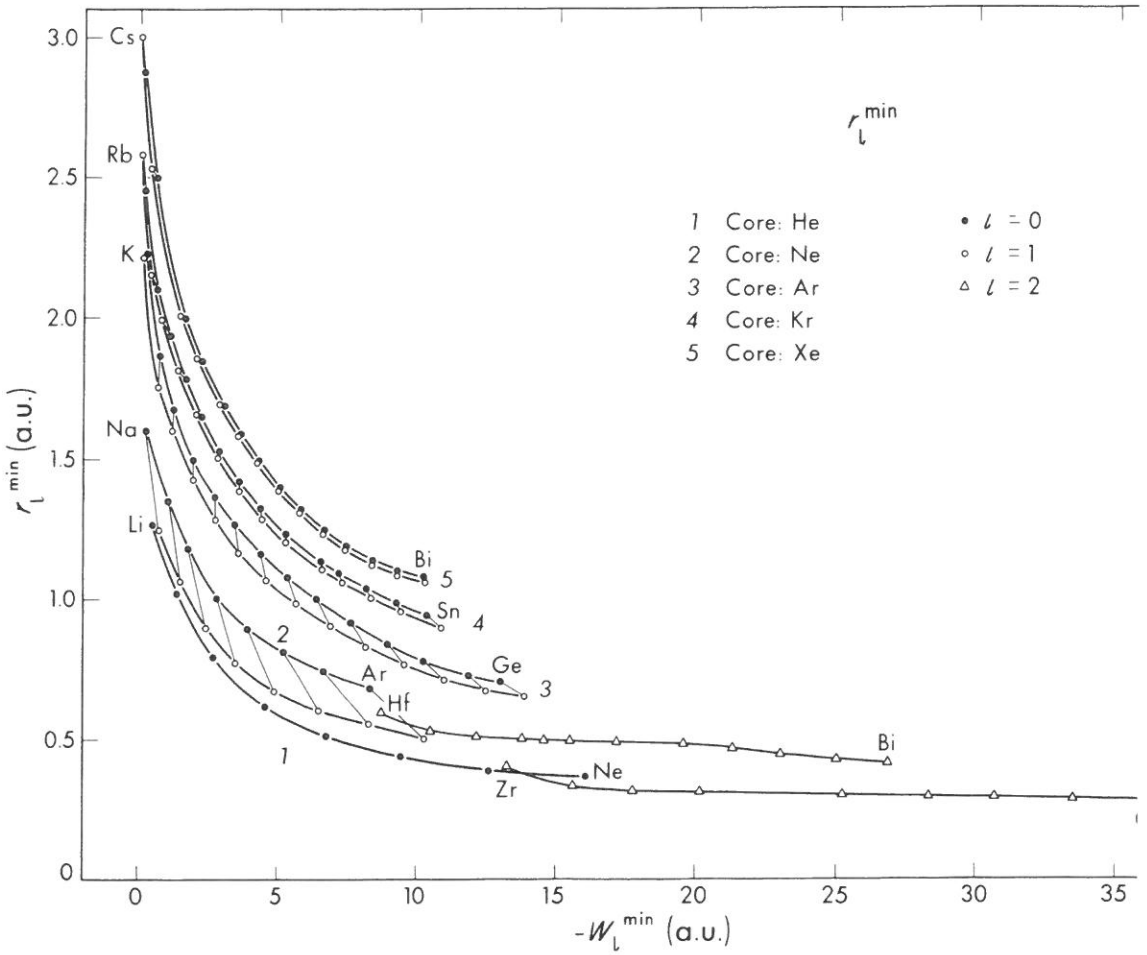

Fig. 9. The correlation between the radius r_l^{min} at which the pseudopotential $v_{ps}^{(l)}(r)$[Eq. (9))] has its minimum and the depth of the minimum $-W_l^{min}$, arranged according to rows in the periodic table. The first and last elements of each row are denoted by their chemical symbol.

circles passing through the $l = 1$ coordinates. The full triangles denote the $l = 2$ coordinates. The $l = 1$ components of the first-row atoms as well as the $l = 2$ components of the second and third rows are purely attractive (cf. Fig. 4c), and all have a minimum of negative infinity at the origin. For clarity of display, we have connected the $l = 0$ and $l = 1$ coordinate of each atom by a straight line. Clearly, the length and slope of these lines measure the s–p nonlocality of the potential. Few interesting observations can be made. The s–p nonlocality decreases as one moves down the columns in the periodic table, as the ratio of the number of core states of $l = 0$ and $l = 1$ symmetry approaches unity, and $U_l(r)$ becomes approximately l-independent. The adequacy of the early *local* pseudopotential models to describe the low energy electronic excitations of compounds such as GaAs, AlAs, InSb, etc., is reflected in the present theory by the proximity of the $l = 0$ and $l = 1$ coordinates of the corresponding atoms. One further notes that while within a given

row the slope of the line connecting the $(r_0^{\min}, W_0)$ and $(r_1^{\min}, W_1)$ coordinates is negative at the right side of each row (i.e., the p potentials are more localized and deeper than the s potentials), these slopes move gradually towards less-negative values and become positive eventually at the left side of the lower rows (i.e., the p potentials become more extended and shallower than the s potentials). This is directly related to the increased delocalization of the outer valence p orbitals as one moves towards the left side of the rows. One notes that the $l = 2$ coordinates are quite separated from the $l = 0$ and 1 coordinates, and vary almost linearly within each row. These localized d potentials are responsible for the relatively narrow and separated d bands in the transition-metal solids. Their variations along the rows parallels the changes in the d-band width in the respective elemental metals, and similarly, their proximity to the $l = 0$ coordinates governs the degree of s–d hybridization.

Having discussed some of the periodic trends exhibited by the atomic pseudopotentials, we now turn to their significance in the establishment of elementary *distance* and *energy* scales, which are quantum-mechanical extensions of similar semiclassical scales discussed in the Introduction.

Figures 10 and 11 display the multiplet-average experimental ionization energy E_l of the atoms (Moore, 1971), plotted against the reciprocal orbital radius r_l^{-1}. For each group of elements, we show two lines: E_s vs. r_s^{-1} and E_p vs. r_p^{-1}. *The striking result is that the theoretical* r_l^{-1} *is seen to form an accurate measure of the experimental orbital energies and hence can be used as an elementary orbital-dependent energy scale*, much like Mulliken's electronegativity. Indeed, since r_l^{-1} is a measure of the scattering power of a screened pseudopotential core towards electrons with angular momentum l, it naturally forms an electronegativity scale. There is an interesting relation between this picture and Slater's concept of orbital electronegativity within the density-functional formalism (Slater, 1974). In his approach, the spin-orbital electronegativity X_i is defined as the orbital energy ε_i of the density-functional Hamiltonian, which in turn equals the derivative of the total energy E with respect to the ith orbital occupation number: $X_i = \varepsilon_i = \partial E/\partial n_i$. In the limit where E is a quadratic function of n_i, this orbital electronegativity reduces to Mulliken's form. This definition is based on the notion that a chemical reaction takes place when electrons will flow from the highest occupied orbitals of a reactant to the lowest unoccupied orbitals with which a finite overlap occurs. Since the present r_l^{-1} coordinate scales approximately with the orbital energy ε_l, the former coordinate is a realization of Slater's electronegativity in a pseudopotential representation.

The orbital radii r_l also form an interesting distance scale (A. N. Bloch, unpublished results, 1980). Consider an all-electron valence atomic wavefunction such as the 4s and 5s orbitals of V and Nb, respectively, depicted in Fig. 12. These wavefunctions have their outer maxima at the points

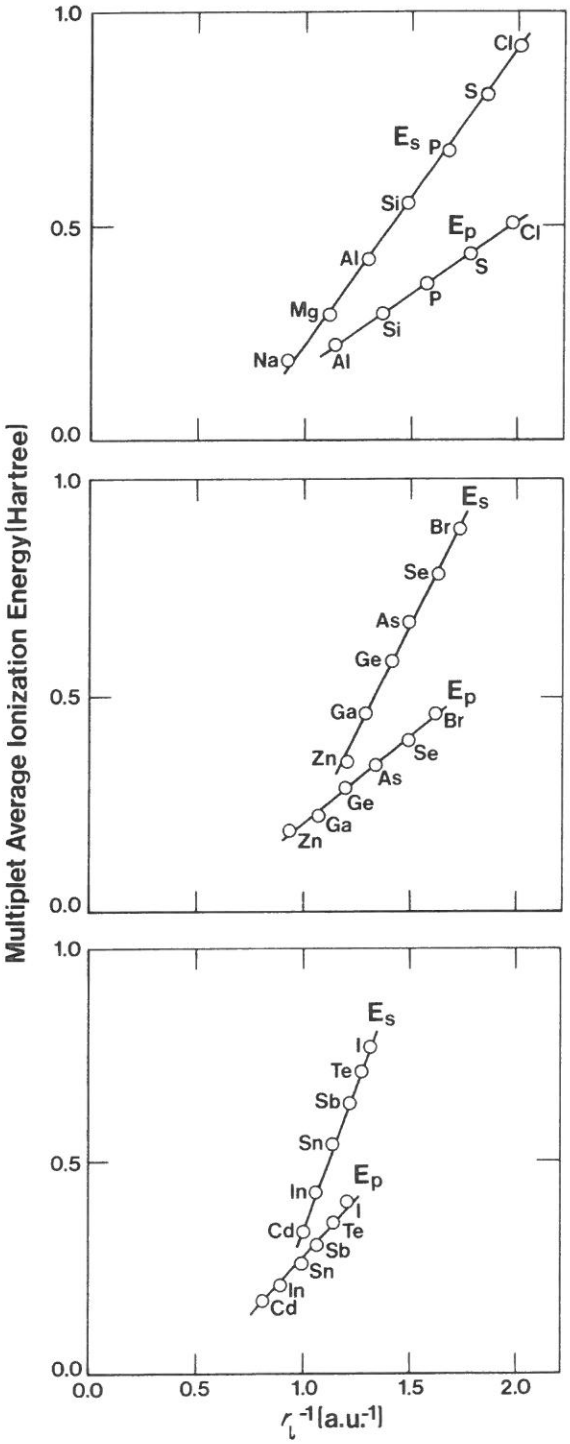

Fig. 10. The correlation between the observed lth orbital multiplet-averaged ionizatioı energies E_l and the reciprocal orbital radius r_l^{-1} (Table I) for the polyvalent elements.

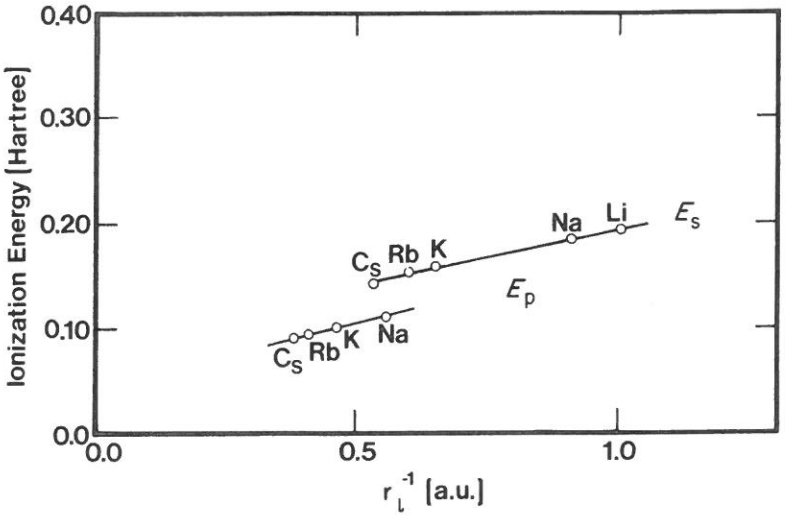

Fig. 11. The correlation between the ground-state (E_s) and excited-state (E_p) orbital ionization energies of the alkali atoms and the corresponding reciprocal orbital radius r_l^{-1} (Table I).

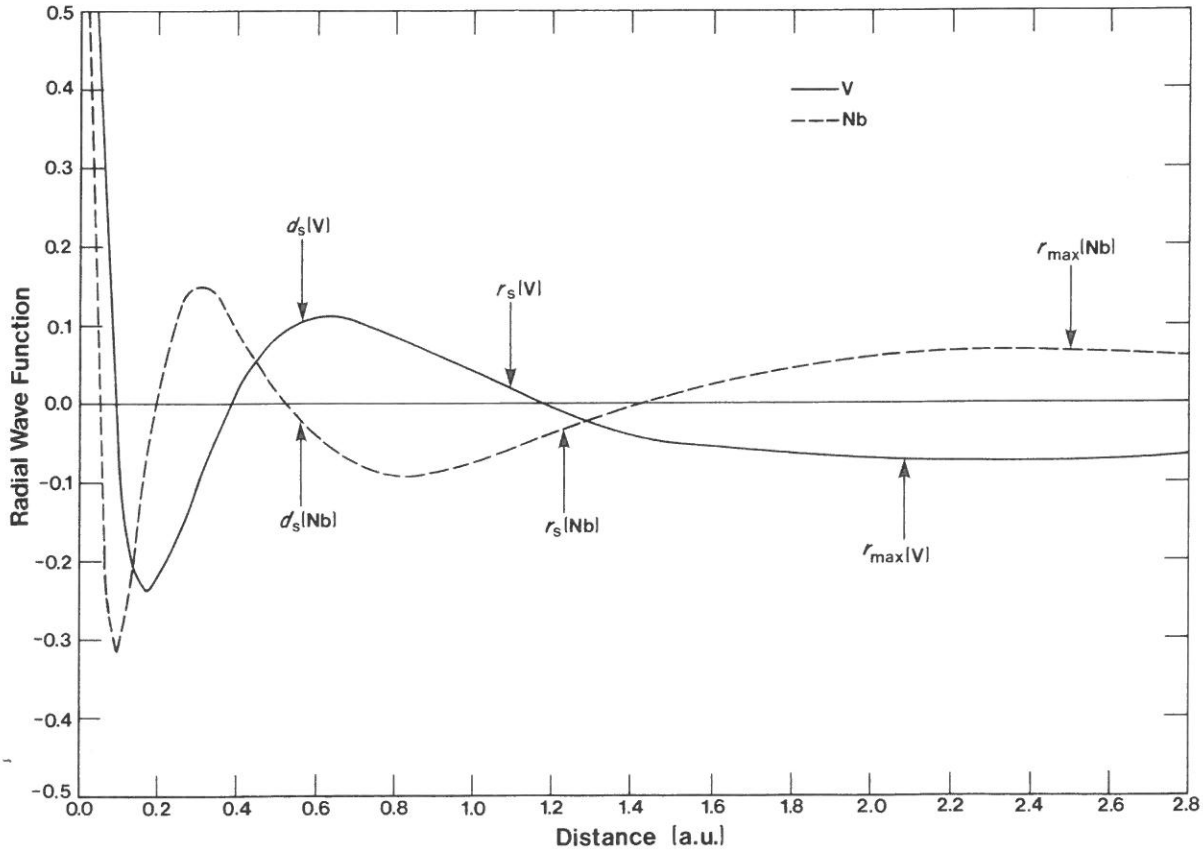

Fig. 12. Radial s-type all-electron wavefunctions for V and Nb: r_{max} denotes the position of the outer orbital maxima, r_s is the screened pseudopotential radius, and d_s is the average node position. Note that r_s is pinned inwards of the last node and outwards of d_s.

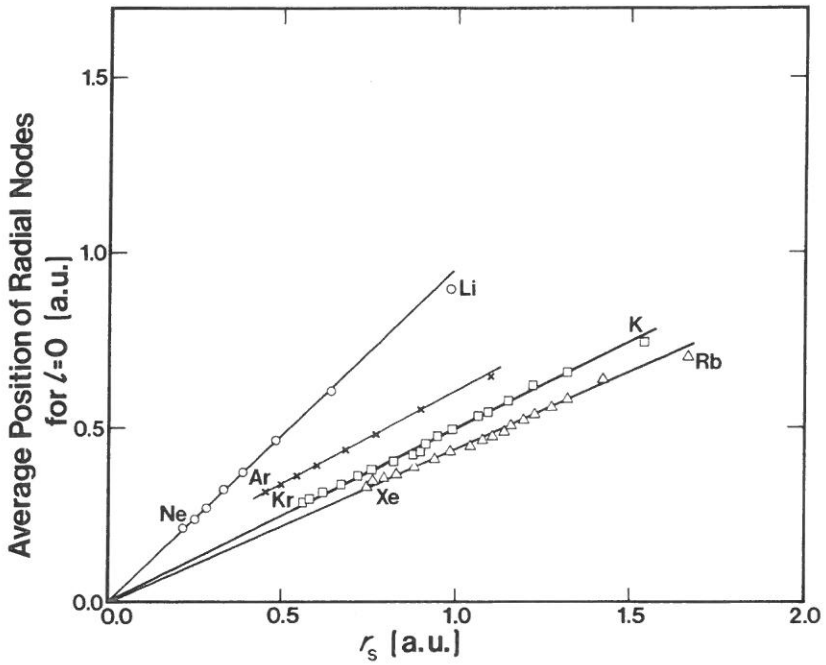

Fig. 13. Correlation between the average node position in the valence all-electron s wave function and the screened pseudopotential radius r_s (Table I). The first and last atom of eacl row are denoted by chemical symbols.

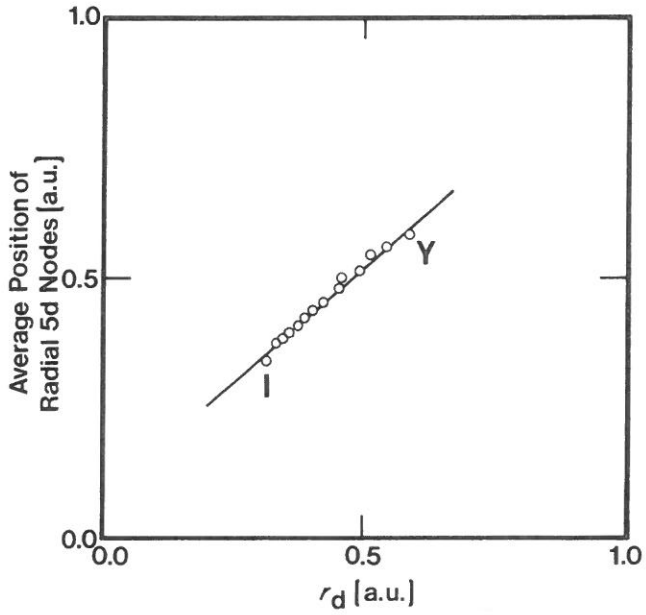

Fig. 14. Correlation between the average node position in the valence all-electron c wavefunction and the screened pseudopotential radius r_d (Table I) for the 4d elements.

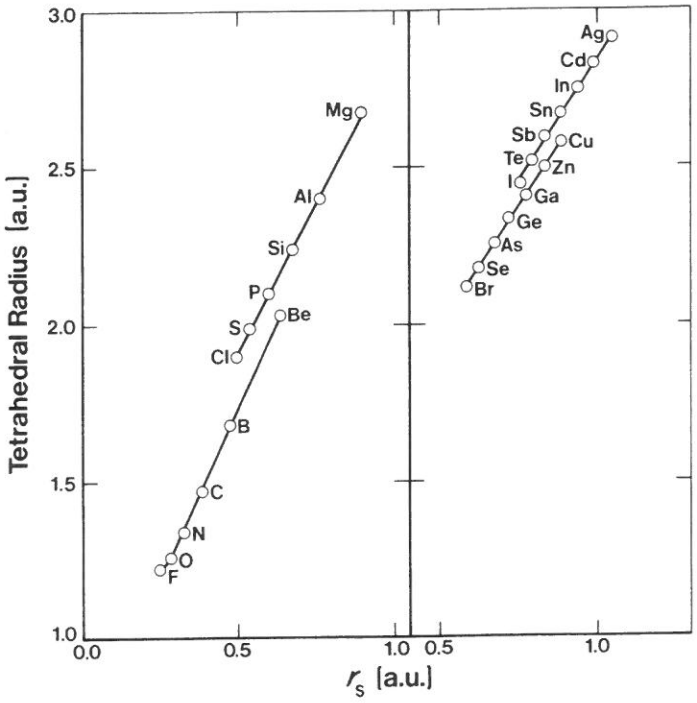

Fig. 15. Relation between Pauling's tetrahedral radius and the s-orbital radius of the screened pseudopotential (Table I).

denoted by r_{max} and have a number of nodes inwards to r_{max}. An algebraic average taken for all node positions in each wavefunction shows that these average positions (denoted by d_l) *are pinned at a certain distance from the orbital radius* r_l. Figure 13 shows the average node position d_l of the outer all-electron s-type valence orbital plotted against r_l, and Fig. 14 shows similar results for d-orbitals (only the first and last element of each row are denoted by the chemical symbol). We find that the oribital radius r_l scales linearly with the average node position, where the row-dependent scale factor increases monotonically with the position of the period in the table of elements (e.g., the scale equals 1.0, 1.5, 2.0, 2.3, and 2.7 for periods 1–5, respectively). *It is seen that the orbital radii* r_l *form, therefore, an intrinsic length scale in that they carry over from the "true" wavefunctions the information on the average node position.* Hence, the dual coordinates $\{r_l, r_l^{-1}\}$ satisfy the semiclassical ideas underlying many successful structural factors (e.g., Pearson, 1972; Hume-Rothery and Raynor, 1954; Pauling, 1960) in forming elementary energy and length scales.

An additional intriguing feature of these orbital radii is their simple correlation with Pauling's tetrahedral radii (Pauling, 1960). As seen in Fig. 15, the tetrahedral radii can be identified with the r_s coordinate to within a row-dependent scale factor.

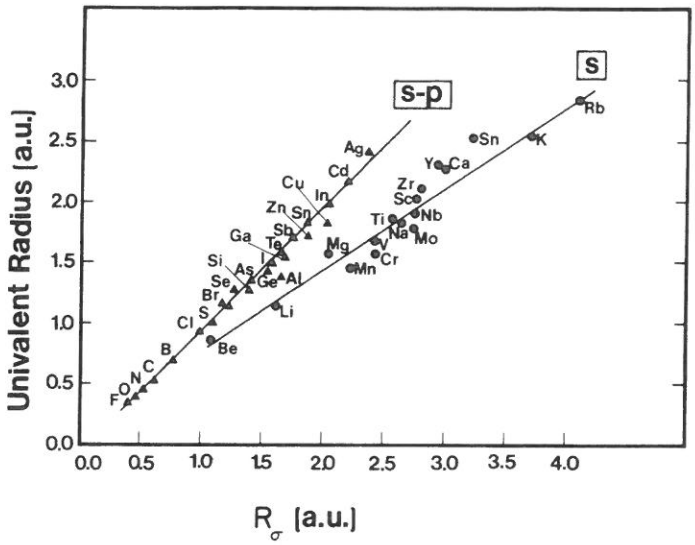

Fig. 16. Relation between Pauling's univalent radii and the total s–p screened pseud potential radius $R_\sigma = r_p + r_s$. Note that this R_σ scale separates the univalent radii into a grou of predominantly s-bonding elements (full circles) and s–p bonding elements (full triangles).

While the individual r_s and r_p radii measure the effective extent of th quantum cores of s and p symmetry, the sum $R_\sigma^A = r_s^A + r_p^A$ provides a mea sure of the total size of the effective core of atom A. Figure 16 depicts R_σ^A versu Pauling's univalent radii for the first three periods of the table of element A similar correlation exists with Gordy's covalent radius (Gordy, 1946 R_σ^A closely follows the regularities of the univalent radii, including thei discontinuity at the end of the transition elements. Examination of Fig. 1 reveals that the present R_σ^A coordinate provides a natural separation o Pauling's univalent radii into those that pertain to atoms sustaining s–p covalently bonded compounds and those in which the s-electrons largel dominate the structural properties. It is remarkable that the orbital radi derived from a pseudopotential formulation of *atomic physics* provide such a close reproduction of the length scale derived experimentally from *solid-stat physics* (e.g., the empty-core radii in Fig. 8, and Pauling's tetrahedral an univalent radii in Figs. 15 and 16, respectively).

We have concentrated in this section on revealing the most significan correlations between the orbital radii and some *transferable* (rather tha compound-dependent) semiclassical coordinates. We will not describ correlations with compound-dependent physical properties (e.g., meltin points, deviations from ideal c/a ratio in Wurtzite structures, elastic constants etc.) not only because this may be too excessive, but also because we believ that many more such interesting correlations are likely to be discovered ir the future. Such correlations between atomic $\{r_l\}$ values and physical prop-

erties $G_{AB}^{(1)}$, $G_{AB}^{(2)}$, etc., may not only serve to systematize those properties but could also point to the underlying dependencies between the seemingly unrelated physical observables $G_{AB}^{(1)}$, $G_{AB}^{(2)}$, etc.

B. Screening Length and Orbital Radii

One can view the quantity r_l^{-1} as being an orbital-dependent screening constant pertinent to the scattering of valence electrons from an effective core. For the nontransition elements, one finds, as expected, that r_l^{-1} falls off monotonically with decreasing valence charge Z_v, reflecting a more effective screening. However, for the 3d, 4d, and 5d transition series (Fig. 17), one finds two distinct behaviors: although r_d^{-1} is a simple, monotonic function, both r_s^{-1} and r_p^{-1} show a break at the point where the d shell is filled. This is intimately related to a similar trend in the orbital shielding constants Z_l^* calculated by Clementi and Roetti (1974) as a rigorous extension of Slater's screening rules. As seen in Fig. 18, the reciprocal screening lengths $(Z_l^*)^{-1}$ for the 3d transition series show a characteristic break around Cu–Zn, much like the corresponding reciprocal radii r_l^{-1}. In constrast, $(Z_l^*)^{-1}$ for the nontransition elements follow a linear trend.

This dual behavior of r_l^{-1} separates the predominantly d-screening domain of the transition elements from the s–p screening domain of the posttransition elements. Note that r_l^{-1} and Z_l^* show uniquely this dual behavior, whereas most chemical and physical quantities are simple monotonic functions of the atomic position in these rows. It is interesting to note that such effects are clearly manifested by s and p coordinates rather than by the d coordinate. This has a central role in the structural significance of the s–p coordinates even for compounds containing transition elements.

C. Comparison with Other Orbital Radii

Figure 19 compares the empirical stripped-ion radii of Simons and Bloch (SB) with the present theoretical values of the density-functional orbital radii for the 41 nontransition elements calculated by SB. The latter set has recently been corrected for the posttransition elements (A. N. Bloch, unpublished results, 1980) relative to the set used by Chelikowsky and Phillips (1978) and Machlin *et al.* (1977). Figure 19 includes the corrected values (e.g., the $l = 0$ crossing-point radii for Cu, Ag, and Au are 0.38, 0.44, and 0.41 a.u., instead of 0.21, 0.22, and 0.13 a.u., respectively). These large corrections change quantitatively some of the results of these previous authors in analyzing the non-octet crystal structures and regularities of melting

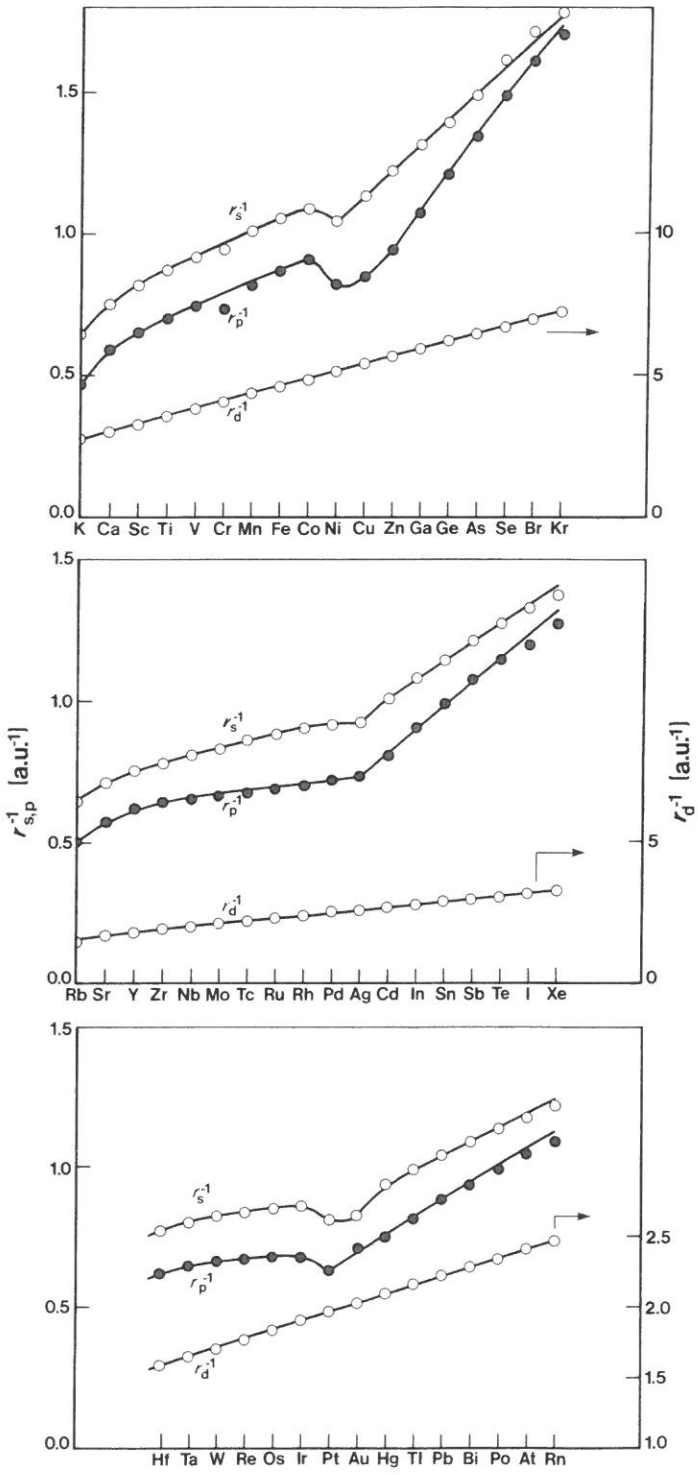

Fig. 17. The regularities in the orbital electronegativity parameters r_l^{-1} (Table I) for the 3d 4d, and 5d transition series. Note the linearity of the r_d^{-1} scale compared with the break in th r_s^{-1} and r_p^{-1} scales.

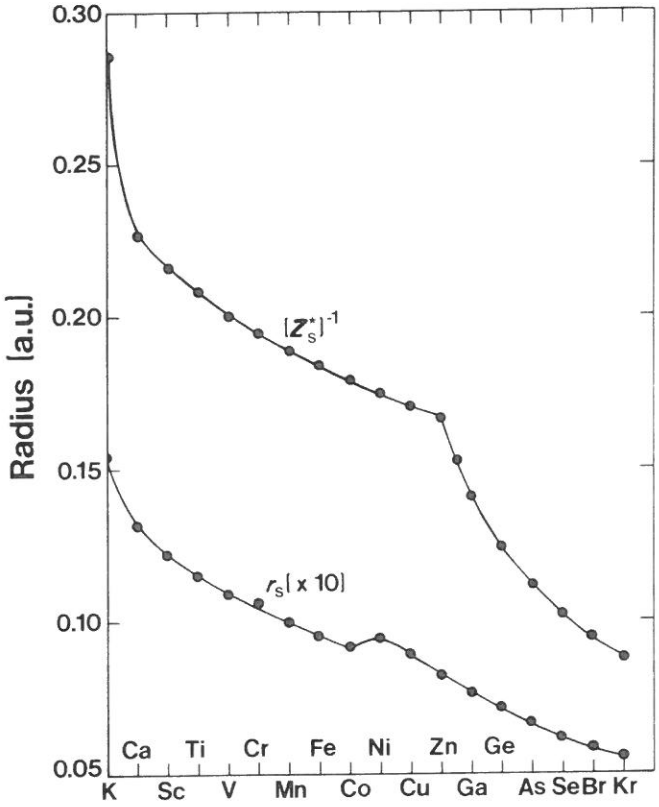

Fig. 18. The regularities in the reciprocal orbital shielding constants $(Z_s^*)^{-1}$ [Clementi and Roetti (1974)] for the third-row elements, compared with the screened pseudopotential radii r_s. Note the break at the end of the transition series.

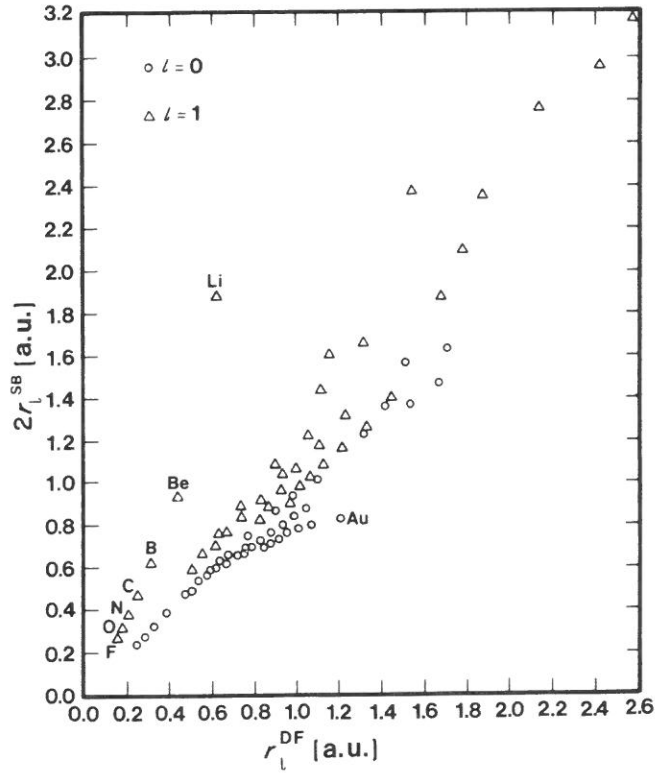

Fig. 19. Correlation between the Simons–Bloch empirical orbital radii r_l^{SB} and the present screened pseudopotential density-functional radii r_l^{DF} (Table I) for the 41 nontransition elements given by Simons and Bloch. The $l = 1$ coordinates of the first-row elements and the $l = 0$ coordinate of Au showing the largest spread, are denoted by their chemical symbol.

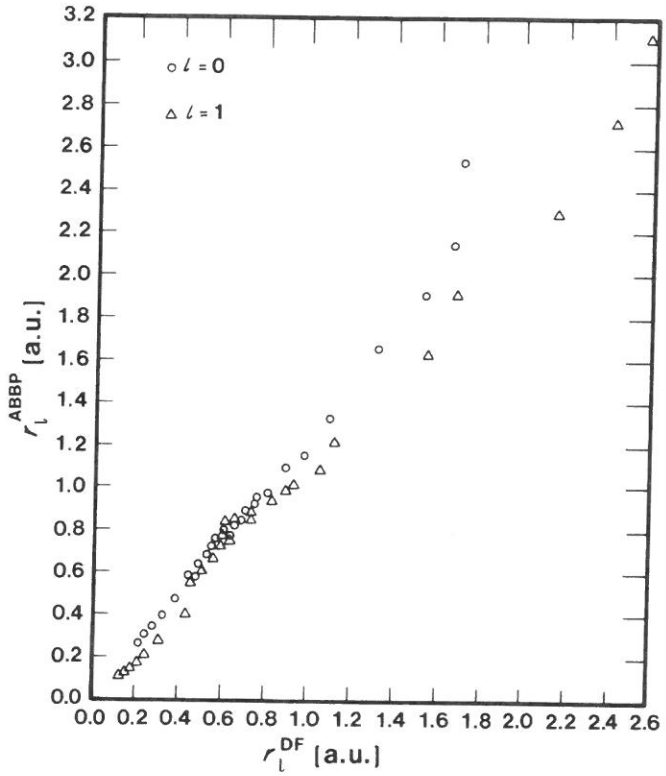

Fig. 20. Correlation between the Anderoni *et al.* (1979) orbital radii r_l^{ABBP} and the presen screened pseudopotential density-functional radii r_l^{DF} (Table I) for the 27 nontransition element given by ABBP.

temperatures, as well as the decomposition of Miedema's heat of formatio model into elemental orbital radii.

Figures 20 compares the recent orbital radii developed by Andreoni Baldereschi, Biemont, and Phillips (ABBP; see Andreoni *et al.*, 1978, 1979 with the present orbital radii, for the 27 nontransition elements calculatec by ABBP. The ABBP radii are obtained from a two-parameter fit of both the Hartree–Fock stripped-ion orbital energies as well as the peak position of the orbital wavefunctions. The values for the eight 3d transition elements given by ABBP are not included in Fig. 20 since, as indicated by these authors, and as we confirm, they are not as reliable.

It can be seen that although the empirical SB radii correlate overall with the present radii, the scatter is fairly large. In particular, the SB scheme predicts $r_s \ll r_p$ for the first-row elements, whereas the present and the ABBP scheme, which attempt to reproduce both energies and wavefunctions, show $r_s > r_p$. The ABBP radii correlate well with our radii (Andreoni *et al.*, 1979) for the 27 nontransition elements. Other plots (e.g., correlation of $|r_s^A - r_p^A|$ or $|r_s^A + r_p^A|$ between the various schemes) lead to similar conclusions.

V. SEPARATION OF CRYSTAL STRUCTURAL OF 565 BINARY AB COMPOUNDS

The orbital radii $\{r_l\}$ derived here can be applied to predict the stable crystal structure of compounds in the same was as discussed by St. John and Bloch (1974), Machlin *et al.* (1977), and Zunger and Cohen (1978a). Having, however, the orbital radii of all atoms belonging to the first five rows in the periodic table, this theory can be applied to a far larger data base of crystals (565) than has been attempted previously (50–80).

Our first step was to compile a list of binary AB compounds whose atoms belong to the first five rows of the periodic table. We were interested in the most stable crystal form of each compound and in a structure that appears in the phase diagram at (or close to) a 50%–50% composition. We started the compilation by reviewing standard tables: Pearson's "Handbook of Lattice Spacings and Structures of Metals and Alloys" (1967); Hultgren *et al.*, "Selected Values of Thermodynamic Properties of Binary Alloys" (1973); Wykoff, "Crystal Structure" (1963); Schubert, "Kristallstrukturen Zweikomponentiger Phasen" (1964); Landolt- Börnstein,"Structure Data of Elements and Intermetallic Phases" (1971); Hansen, "Constitution of Binary Alloys" (1958); Rudman *et al.*, "Phase Stability in Metals and Alloys" (1966); Pearson, "The Crystal Chemistry and Physics of Metal and Alloys" (1972); and Parthé, "Crystal Chemistry of Tetrahedral Structures" (1964); as well as a number of basic papers, such as Rieger and Parthé (1966), Schob and Parthé (1964), and Schubert and Eslinger (1957), which give useful tables for particular structures. Whenever we have identified in this literature either a conflict in assigning a crystal structure or expressions of doubt as to the identification of the structure, other structures at somewhat different pressures or temperatures, substantial deviation from 1:1 stoichiometry, etc., we have made use of a computer-assisted literature search to find the original papers for the compounds in question. In this way, we have surveyed some 180 references. We have identified from standard sources as well as from an extended computer search a total of about 565 binary AB compounds that are near-stoichiometric, ordered, and formed from atoms belonging to the first five rows of the periodic table. Their distribution among the various crystal structures is given in Table IV.

This data base of 565 binary compounds exhibits an enormous range of physical, structural, and chemical properties. Using the terminology of the semiclassical structural factors, one notes the large range of conductivity properties spanned by these compounds (insulators, semiconductors, semimetals, metals, superconductors), the electronegativity difference (covalent vs. large ionicity), coordination numbers (12 to 2), relative ionic sizes of the

TABLE IV

AB Crystal Structures Used in the Structural Plots[a]

Strukturberichte or Pearson symbols	Space group	Unit cell	Prototype	Number of compounds
		Octet		
B1	$Fm3m$	cubic	NaCl	65
B2	$Pm3m$	cubic	CsCl	3
B3	$F\bar{4}3m$	cubic	ZnS	29
B4	$P6_3mc$	hexagonal	ZnO	11
A4	$Fd3m$	cubic	diamond	4
Total				112
		Non-octet		
B1	$Fm3m$	cubic	NaCl	33 + 8
B2	$Pm3m$	cubic	CsCl	122 + 2
$B8_1$	$P6_3/mmc$	hexagonal	NiAs	62 + 3
B10	$P4/nmm$	tetragonal	PbO	0 + 2
B11	$P4/nmm$	tetragonal	CuTi	7
B16	$Pnma$	orthorombic	GeS	0 + 7
B19	$Pmma$	orthorombic	CuCd	11
B20	$P2_13$	cubic	FeSi	17
B27	$Pnma$	orthorombic	FeB	16
B31	$Pnma$	orthorombic	MnP	30
B32	$Fd3m$	cubic	NaTl	7
B33	$Cmcm$	orthorombic	CrB	41
B35	$P6/mmm$	hexagonal	CoSn	3
B37	$I4/mcm$	tetragonal	SeTl	0 + 3
B_h	$P\bar{6}m2$	hexagonal	MoP	4
cP64	$P43n$	cubic	KGe	6
hP24	$P6_3/mmc$	hexagonal	LiO	3
$L1_0$	$P4/mmm$	tetragonal	CuAu	27
mC24	$c2/m$	monoclinic	AsGe	0 + 4
mC32	$C2/c$	monoclinic	NaSi	1
mP16	$P2_1/c$	monoclinic	AsLi	4
mP32	$P2_1/n$	monoclinic	NS	0 + 5
oC16	$Cmcm$	orthorombic	NaHg	1
oC16	$Cmca$	orthorombic	KO	1
oC48	$Cmc2_1$	orthorombic	SiP	0 + 1
oI8	$Immm$	orthorombic	RbO	4
oP16	$P2_12_12_1$	orthorombic	NaP	6
tI8	$I4/mmm$	tetragonal	HgCl	0 + 3
tI32	$I4_1/a$	tetragonal	LiGe	1
tI32	$I4/mcm$	tetragonal	TlTe	0 + 1
tI64	$I4_1/acd$	tetragonal	NaPb	7
Total				453

[a] When two entries appear for the number of compounds, the first indicates the number of suboctet compounds and the second denotes the number of non-transition-element suberoctet compounds.

A and B atom, bonding type (covalent, ionic, metallic, etc.), range of heats of formation ($\simeq 1-150$ kcal/mole), electron per atom ratios ($\simeq 1.5$ to $8-9$), etc. Given this distribution of the 112 octet compounds and 453 non-octet compounds into 5 and 31 different crystal structures, respectively exhibiting a diverse range of properties, we now ask how well can the atomically derived orbital radii scheme explain such a distribution.

We construct from the s and p atomic orbital radii the dual coordinates for an AB compound as:

$$\begin{aligned} R_\sigma^{AB} &= \left|(r_p^A + r_s^A) - (r_p^B + r_s^B)\right| \\ R_\pi^{AB} &= \left|r_p^A - r_s^A\right| + \left|r_p^B - r_s^B\right| \end{aligned} \tag{23}$$

Here, R_σ^{AB} is a measure of the different between the total effective core radii of atoms A and B (i.e., size mismatch); whereas R_π^{AB} measures the sum of the orbital nonlocality of the s and p electrons on each site. Using the definition [Eq. (23)] and the values of the orbital radii given in Table I, we construct R_σ^{AB} vs. R_π^{AB} maps for the binary compounds. Such maps are shown for 112 octet compounds in Fig. 21 and for 356 of the non-octet compounds

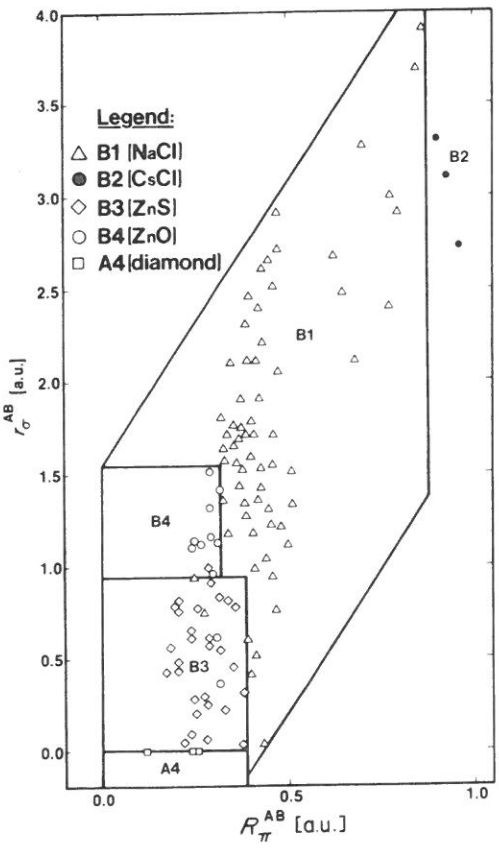

Fig. 21. A structural separation plot for the 112 binary octet compounds, obtained with the density-functional orbital radii, with $R_\sigma^{AB} = |(r_p^A + r_s^A) - (r_p^B + r_s^B)|$, $R_\pi^{AB} = |r_p^A - r_s^A| + |r_p^B - r_s^B|$.

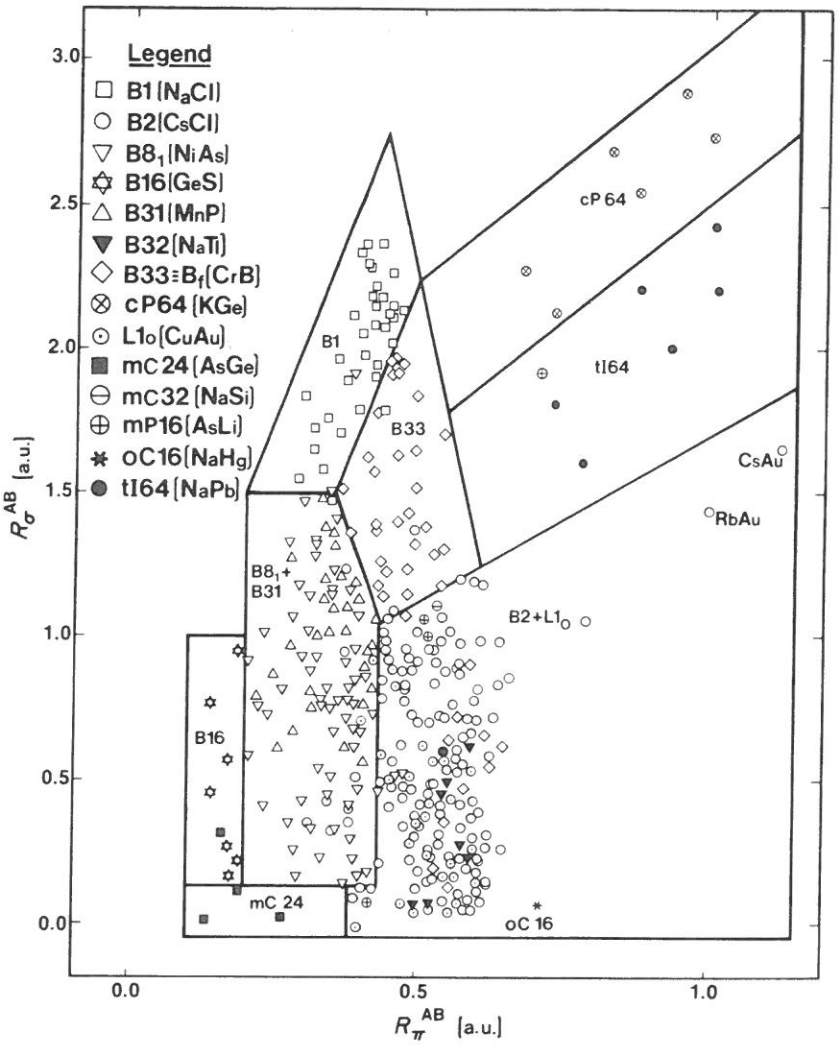

Fig. 22. A structural separation plot for the 356 binary non-octet compounds, obtaine with the density-functional orbital radii, with $R_\sigma^{AB} = |(r_p^A + r_s^A) - (r_p^B + r_s^B)|$, $R_\pi^{AB} = |r_p^A - r_s^A| - |r_p^B - r_s^B|$.

in Fig. 22. (For example, for NiAs, we have from Table I: $r_s^{Ni} = 0.96$ a.u., $r_p^{Ni} = 1.22$ a.u., $r_s^{As} = 0.67$ a.u., and $r_p^{As} = 0.745$ a.u.; hence, $R_\sigma^{NiAs} = (1.22 + 0.96) - (0.745 + 0.67) = 0.765$ a.u. and $R_\pi^{NiAs} = (1.22 - 0.96) + (0.745 - 0.67) = 0.335$ a.u. This appears in the B8$_1$ domain in Fig. 22.)

We identify each structure by a different symbol and search for the smalles number of straight lines, enclosing minimal areas, best separating the differen structures. In some cases, there exists a unique solution to this topologica problem; in other cases (e.g., B33 and cP64 and tI64 structures), there ar a number of permissible solutions. However, in these cases it seems to mak little difference which line is chosen. While we could have lowered the numbe of "misplaced" compounds by using more complex lines, we feel that th

more stringent criterion of using straight lines provides us with a better chance of assessing the true success of the method.

The remarkable result of these plots is that with *the same linear combination of atomic orbital radii*, most of the structures to which the 468 compounds appearing in these plots belong can be separated. The relative locations of the structural domains seems chemically reasonable. Hence, the B27–B33 (coordination number CN = 7) is intermediate between the B1 structure (CN = 6) and the B2–$L1_0$ structures (CN = 8). The mostly metallic non-octet compounds appear separate from the nonmetallic regime to the right (cP64, tI64, mC32, mP16, oC16), etc. Within single structural groups one similarly finds a chemically reasonable ordering of compounds,—e.g., polymorphic compounds (such as SiC) appear near border lines, Zinc blende–rock salt pairs that intertransform at low pressure appear along their separating line, etc. Note that even the wurtzite–zinc blende structures, which only differ starting from the third nearest-neighbors, are well separated. However, there are a number of crystallographically closely related structures that overlap: I am unable to separate the non-octet crystal type (B2) from the CuAu (Ll_0 structure), the NiAs-type ($B8_1$) from the MnP-type (B31), and the CrB type (B33) from the FeB type (B27), etc. For charity of display, I show some of the extra overlapping structures separately in Fig. 23, *using, however, precisely the same separating lines as used for all other non-octet compounds (Fig. 22)*.

It is not surprising that some of these structural pairs overlap. For instance, the B27 and B33 structures have a common structural unit consisting of a row of trigonal prisms of atom A stacked side by side and centered by a zigzag chain of B atoms (Hohnke and Parthé, 1965). The structural similarity between CsCl (B2) and CuAu ($L1_0$) has been discussed by Hume-Rothery and Raynor (1954); the relation between the NiAs ($B8_1$), MnP (B31), and the FeSi (B20) structures by Schubert and Eslinger (1957); and that between the CsCl (B2), AuCd (B19), and CuTi (B11) by Pearson (1972). In fact, examination of the thermochemical data (Hultgren *et al.*, 1973; Kubaschewski and Alcock, 1979, and references therein) indicates that if a certain compound exists in two of these related structures at somewhat different temperature, the difference in their standard heats of formation is often as small as 0.3 kcal/mole! (For example, AgCd in the B19 structure has $\Delta H = 0.094 \pm 0.004$ eV, whereas the B2 structure has a heat formation of 0.080 ± 0.004 eV.) Also, some of these presently unseparated structures indeed appear as mixtures when prepared from the melt [e.g., as noted by Honke and Parthé (1965), both the B27 and B33 structures are frequently found in the same arc-melted buttons of these compounds].

Since the publication of a preliminary report of this work (Zunger, 1980d), which included 495 compounds, I have been made aware of the crystal

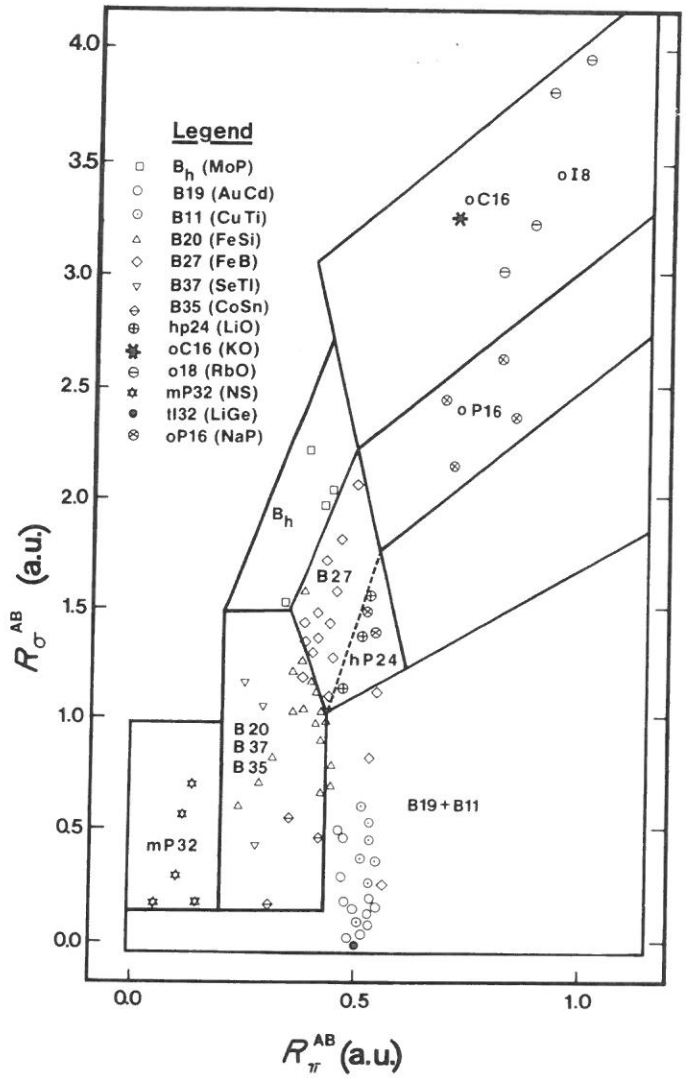

Fig. 23. A structural separation plot for the 81 binary non-octet compounds, obtained with the density-functional orbital radii, with $R_\sigma^{AB} = |(r_p^A + r_s^A) - (r_p^B + r_s^B)|$, $R_\pi^{AB} = |r_p^A - r_s^A| + |r_p^B - r_s^B|$.

structures of 54 more octet and suboctet compounds as well as 16 new superoctet compounds (i.e., a total of 565 compounds). I find that the lines separating the structural domains of the octet and suboctet compounds need not be changed relative to their previous assignment to incorporate the 54 new compounds. All the superoctet compounds (a total of 34) could be separated clearly as well (Fig. 24 and discussion below). This illustrates the predictive ability of the present approach.

If one is to consider the pairs of related crystal structures mentioned above as belonging to single generalized structural groups, the total number of misplaced compounds (5 octet and 32 non-octet) forms only 7% of the total

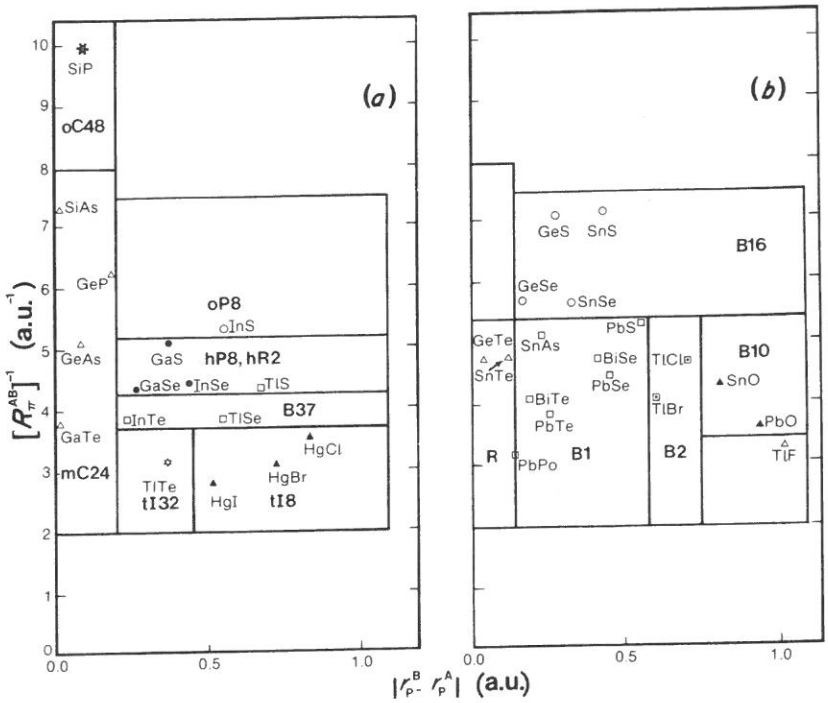

Fig. 24. A structural separation plot for the 34 superoctet compounds $A^N B^{(10-N)}$ with valence electron concentrations VEC = 9 (Fig. 24*a*) and 10 (Fig. 24*b*). The structural groups are defined in Table IV. The symbol *R* (Fig. 24) denotes a romboledral structure. In the B1 domain of Fig. 24*b* we have also included the compounds with VEC = 9, 11.

data base of binary compounds. In this respect the present theory is more than 90% successful.

The compounds that are "misplaced" in the present theory (i.e., their $\{R_\sigma^{AB}, R_\pi^{AB}\}$ coordinates place them in a different structural domain than that reported in the literature surveyed) are listed in Table V together with their $\{R_\sigma^{AB}, R_\pi^{AB}\}$ coordinates. In cases where a compound appears in overlapping domains or close to a border line, we indicate all the pertinent structures. Given their $\{R_\sigma^{AB}, R_\pi^{AB}\}$ coordinates, the reader can conveniently identify them on structural plots.

The list of misplaced compounds shows a number of interesting features. At least two compounds, CuF and FeC, reported to have the B3 and B1 structures, respectively, probably do not exist at all (for CuF see Barber *et al.*, 1961; for FeC, F. Jellenek, private communication, 1980). Their "misplacement" in the present theory is hence a graftying feature.

Similarly, while OsSi (No. 11) is sometimes reported to have the B2 structure (e.g., Landolt-Bornestein, 1971) and appears in our plots in the B20 domain (No. 11 in Table 5), it is known to actually have the B20 structure and appears in B2 only with impurities. In addition, the compound PtB (No. 18 in Table V) which has been reported to have the NiAs ($B8_1$) structure and is placed in our plots in an entirely unrelated structural domain, has been found to have an anti-NiAs structure. NiY (No. 30) was reported in

TABLE V

Compounds Which are Misplaced in the Present Theory (out of a Total of 565)

Compound	Expected structure	Structural domain(s) in which it is found	R_σ^{AB} (a.u.)	R_π^{AB} (a.u.)
		Octet		
1. CuF	B3	B1	1.635	0.375
2. MgS	B1	B3	0.93	0.25
3. BeO	B4	B1–B3	0.615	0.305
4. MgTe	B4	B1–B3	0.36	0.32
5. MgSe	B1	B1–B3–B4	0.745	0.285
		Non-Octet		
1. CoAl	B2	$B8_1$–B31–B20	0.345	0.315
2. FeAl	B2	$B8_1$–B31–B20	0.435	0.345
3. NiAl	B2	$B8_1$–B31–B20	0.505	0.395
4. CoGa	B2	$B8_1$–B31–B20	0.325	0.355
5. FeGa	B2	$B8_1$–B31–B20	0.415	0.385
6. NiGa	B2	$B8_1$–B31–B20	0.485	0.435
7. NiIn	B2	$B8_1$–B31–B20	0.13	0.43
8. MnIn	B2	$B8_1$–B31–B20	0.17	0.41
9. CoPt	$L1_0$	$B8_1$–B31–B20	0.68	0.40
10. TiAl	$L1_0$	$B8_1$–B31–B20	0.905	0.415
11. OsSi	B2	$B8_1$–B31–B20	1.23	0.37
12. CoBe	B2	$B8_1$–B31–B20	0.94	0.38
13. PdBe	B2	B33–B27	1.37	0.49
14. NaPb	tI64	B2–$L1_0$–B32	0.56	0.52
15. AuBe	B20	B1–B33–B27	1.58	0.44
16. FeC	B1	B1–$B8_1$–B31	1.47	0.35
17. TiB	B1	B1–B33–B27	1.785	0.445
18. PtB	$B8_1$	B1–B33–B27	1.905	0.385
19. IrPb	$B8_1$	$B8_1$–B31–B2	0.538	0.478
20. AgCa	B33	B1–$L1_0$	0.625	0.645
21. HfPt	B33	B2–$L1_0$	0.21	0.53
22. NiHf	B33	B2–$L1_0$	0.73	0.57
23. NiLa	B33	B2–$L1_0$	0.90	0.59
24. NiZr	B33	B2–$L1_0$	0.645	0.555
25. PtLa	B33	B2–$L1_0$	0.38	0.55
26. RhLa	B33	B2–$L1_0$	0.56	0.63
27. ZrPt	B33	B2–$L1_0$	0.125	0.515
28. PdLa	B33	B2–$L1_0$	0.63	0.62
29. AuLa	B27–B33	B2–$L1_0$	0.42	0.57
30. NiY	B27	B2–$L1_0$	0.76	0.56
31. PtY	B27	B2–$L1_0$	0.24	0.52
32. LaCu	B27	B2–$L1_0$	1.04	0.61

1960 (e.g., Elliot, 1965, p. 678) to have the orthorhombic B27 structure, in conflict with the prediction of the present scheme, while in 1964 (e.g., Shunk, 1969, p. 561) it was concluded that it is actually monoclinic with a $P2_1/a$ space group. It seems that no clear identification for this structure is yet available. While HfPt (No. 21) is identified in most sources as having a B33 orthorhombic structure, a deformed B2 modification has also been reported (e.g., Shunk, 1969, p. 419). Similarly, AuBe (No. 15) has been reported in 1947 to have the B20 structure (e.g., Elliot, 1965, p. 83) while in 1962 (e.g., Shunk, 1969, p. 64) it has been identified as tetragonal. AuLa (No. 29) has been reported to transform from its high temperature B33 form to a low-temperature B27 form (both orthorhombic) at about 660°C, while in 1963 (Shunk, 1969, p. 73) it was indicated to have the cubic B2 form. It is hence clear that for some of the "misplaced" compounds, it is not yet obvious whether their misplacement is real. For the other compounds appearing in Table V their misplacement in the present phase diagrams is real and brings up a number of interesting observations.

The octet compounds MgS and MgSe have a NaCl (B1) structure but appear in our plot in the ZnS (B3) domain, near the B1 border. Experimentally (e.g., Navrotsky and Phillips, 1975) it is found that the (normalized) free energy of the B3–B1 phase transition for these compounds is nearly zero.

A large number of the other misplaced compounds have unusual properties. Two such groups of compounds show *systematic* unusual properties: the six Al and Ga compounds with the magnetic 3d transition elements (CoAl, FeAl. NiAl, CoGa, FeGa, and NiGa) and the group of ten CrB and three FeB structures (AgCa, HfPt, NiHf, NiLa, NiZr, PtLa, ZrPt, PdLa, and AuLa, and NiY, PtY, and LaCu, respectively).

The first group has the CsCl (B2) structure but appears in the present theory in the domain of the NiAs–MnP–FeSi structures. Their electric and magnetic properties have been studied intensively in the last few years (e.g., Brodsky and Brittain, 1969; Herget *et al.*, 1970; Wertheim and Wernick, 1967; Huffman 1971; Bose *et al.*, 1979; Müller *et al.*, 1979; Kiewit and Brittain, 1970; Caskey *et al.*, 1972; Sellmyer *et al.*, 1971). It appears that these compounds are stabilized by the presence of defects, and they have a large, stable range of composition (45–55%).

Susceptibility measurements as a function of magnetic field show ferromagnetic impurities and antistructure defects in such materials. More importantly, a slight nonstoichiometry often leads to the formation of local magnetic moments. These results indicate (e.g., Sellmyer *et al.*, 1971) that such slightly off stoichometric materials are in effect spin glasses at low temperatures. Their magnetic behavior is intermediate between that of the independent magnetic impurity problem (Kondo effect) and that characteristic of antiferromagnetic or ferromagnetic systems having long-range

order due to strong magnetic interactions. It is interesting to note that thi subgroup of compounds exhibiting stable intrinsic defects leading to mag netic moments, are displaced in the structural plots from the largely non magnetic B2 domain to the $B8_1$ region in which even the stoichiometri alloys have permanent local moments. There are indications that thi subgroup of compounds have certain structural anomalies: Many author report that the B2 aluminides could not be obtained as a single phase, an in diffraction the B2 pattern could not be separated from other diffractio lines not belonging to this structure (Schob and Parthé, 1964). It was sug gested (Schob and Parthé, 1964) that many of these compounds are onl *metastable* in the B2 structure. In a recent diffraction study (Gerold, 1978 it was discovered that strong distortions occur around Co sublattice site in CoGa due to intrinsic vacancies. Similarly, a recent calculation (Bras *et al.* 1977) of the ordering energy in FeGa, using a Bragg–Williams model, yielde very small interaction parameters of 0.049 eV and 0.03 eV (i.e., $\sim 2-1\ kT$ for first and second neighbors, respectively. It is intriguing that the presen orbital radii scheme has the ability of identifying such unusual phenomena in a few of the 122 tabulated B2 nonoctet compounds.

Our scheme suggests that similar irregularities may occur in NiIn and TiAl and perhaps even in CoBe, but to a much smaller extent, since these compounds are only marginally misplaced in the present theory. Indeed, the absorption spectra of NiIn in the 0.7–5.5 eV range (Best *et al.*, 1971) indicate almost no change with composition in its Drude regime as well as above it, suggesting constant number of electrons per cell due to the defect structure. This suggests that many of the unusual magnetic and structural properties found in the FeAl, FeGa, CoAl, CoGa, NiAl, NiGa group may may also be found in NiIn.

The second large group of misplaced compounds (numbers 20–32 in Table V) form a distinct structural group. Schob and Parthé (1964), Rieger and Parthé (1966), and Hohnke and Parthé (1965) have indicated that all CrB (B33) and FeB (B27) compounds can be separated into two groups: group I, in which a transition-metal atom combines with an s–p element (B, Si, Ge, Al, Ga, Sn, or Pb), and group II, in which a transition element from the third or fourth group combines either with another transition element from group VIII or from the Cu group. It was found that the individual trigonal prisms in both the FeB and the CrB structures have different relative dimensions in groups I and II. In particular, group I of the CrB structure shows a "normal" a/c ratio greater than one, but group II compounds show a compressed prism with $a/c < 1$. Only three compounds belonging to group I (HfAl, ZrAl, and YAl) have $a/c < 1$. We find that *all of the CrB and FeB compounds that belong to group II are misplaced by our theory into the bordering CsCl domain*, whereas the three group I compounds that have $a/c < 1$

(much like group II compounds) are correctly placed. Hence, the present approach is sufficiently sensitive to separate the true physical irregularity even when simple structural factors such as the a/c ratio lead to the wrong conclusion. From the results of the present approach, it would seem that group II compounds of the FeB and CrB structures should properly be identified as a separate group. As a result, if the errors made by the present theory for the latter group of compounds as well as the errors in the 1–8 (Table V) local-moment materials are regarded as *systematic irregularities*, the remaining "true" errors amount to only 2% of the total data base.

The remaining misplaced compounds may also have unusual properties; NaPb (No. 14) has an unusual structure resembling a molecular crystal with 64 atoms per cell and interacting Pb_4 tetrahedra (Marsh and Shoemaker, 1953; Hewaidy *et al.*, 1964); IrPb (No. 19), according to Miedema's (1976) model, has a positive heat of formation of about 1 kcal/mole.

Similarly AgCa (No. 20) has been recently discovered (Amand and Giessen, 1978 to be one of the only known glass-forming materials that do not contain a transition element. It has also been noted (Chelikowsky and Phillips, 1978 that the ratio of anion–anion to cation–anion distances in AgCa is almost an order of magnitude smaller than in all other nontransition metal B33 compounds and that unlike the latter group of compounds it has catalytic properties in redox reactions.

The relative orientation of the structural domains in Figs. 21–23 suggest that no *single* coordinate will suffice to produce a complete topological separation between all structures. Since, however, the area of the R_σ^{AB} vs. R_π^{AB} plane seems to be more or less bound (e.g., ≈ 3 a.u.^{2} in Fig. 22) when extra compounds are added, it is likely that the two-dimensionality of this finite R_σ^{AB}–R_π^{AB} space will eventually preclude the delineation of further structures. One may hence expect that for some critical number of structures and compounds, a third coordinate may be needed. Such a generalized multidimensional resolution of structural groups may also resolve some of the remaining discrepancies in the present theory. Our present approach however is aimed at demonstrating the extent of structure delineation possible with the minimum number of two coordinates using the simplest possible separating lines.

One simple example for an additional coordinate is the classical (e.g. Pearson, 1969) valence electron concentration VEC, measuring for the binary AB system the total number of valence electrons $Z_v^A + A_v^B$ [c.f. Eq. (9)] in the compound. In the semiclassical approaches to structure it is known that whereas the VEC value alone does not separate different crystal structures, compounds with the same valence electron number often belong to the same broad structural groups. One can use this additional coordinate together with our orbital radii to obtain a better structural resolution of the marginally

resolved structures, and at the same time provide a clear structural delineation of all *superoctet* (i.e., $Z_v^A + Z_v^B > 8$) compounds. As with the suboctet compounds, no previous approach has succeeded in systematizing these complex crystal structures.

We find that while the definition of the structural coordinates R_π^{AB} and R_σ^{AB} [Eq. (23)] used for the octet (Fig. 21) and mostly suboctet (Figs. 22, 23) compounds yields an overall separation also of the superoctet compounds, a more sensitive delineation is obtained with the slightly modified coordinates $R_1 = |r_p^B - r_p^A|$ and $R_2 = (R_\pi^{AB})^{-1}$ suggested by Littlewood (1980). Here, R_1 is a measure of the p-orbital electronegativity difference between atoms A and B, while R_2 measures the s–p nonlocality on the two sites. The reason that $|r_p^B - r_p^A|$ forms a better structural coordinate for superoctet compounds is that these systems involve relatively heavy atoms (e.g., Pb, Sn, Bi, Tl, Hg) for which the s electrons are paired and strongly bound relative to the p electrons. Hence, these semicore s orbitals become chemically inactive and only the contribution of the p electons needs to be included in the electronegativity parameter R_1.

Figures 24*a* and 24*b* show structural plots for the superoctet compounds with 9 and 10 valence electrons respectively. Since there are only a few B1 superoctet compounds, we have included those with VEC = 9 (SnAs), VEC = 10 (PbS, PbSe, PbTe, and PbPo) and VEC = 11 (BiSe, BiTe) on the same plot in Fig. 24*b*. Figure 24 includes 18 compounds which have appeared in the previous nonoctet plots (Figs. 22 and 23): B37 (InTe, TlSe, TlS), mC24 (GaTe, GeAs, GeP, SiAs), B16 (GeS, SnS, GeSe, SnSe, InS), pseudo-$B8_1$ (GaS, GaSe, GeTe, SnTe, InSe), and the orthorombically distorted B1 compound TlF. It is seen that the seven different structures of the VEC = 9 compounds as well as the six different VEC = 10 structures are very clearly resolved, the only exception out of these 34 compounds being the B37 compound TlS which is marginally displaced into the neighboring hP8-hR2 domain (Fig. 24*a*).

It is interesting to note that the present scheme also predicts unusual *electronic properties* of compounds belonging to the same structural group. For instance, the B2 compounds CsAu and RbAu that appear in Fig. 22 as isolated from the other 147 B2 + $L1_0$ compounds have semiconducting properties (e.g., Spicer, 1962), while all other suboctet compounds belonging to these structures seem to be metals. A recent calculation of the electronic band structure of CsAu (Hasegawa and Watabe, 1977) has indicated that if relativistic corrections are neglected, CsAu appears to be a metal, which disagrees with experiment, whereas the inclusion of relativistic effects lowers the Au s valence band to form a semiconductor. It is remarkable indeed that such complicated electronic structure factors are required in quantum-

mechanical band-structure calculations to reveal the unusual semiconducting behavior suggested here simply by the atomic orbital radii.

If the predictive power of the present orbital radii scheme in relation to unusual electronic properties is not accidental, it would be interesting to speculate on its consequences. One would guess, for instance, that all *sub-octet nontransition element* compounds having R_π^{AB} larger than roughly 0.7 a.u. are nonmetals! This includes not only the known nonmetallic compounds belonging to the LiAs group (KSb, NaGe, NaSb, but not LiAs) and the KGe group (CsGe, CsSi, KGe, RbGe, and RbSi, whereas KSi is a borderline case), but also the tI64 (NaPb) group (CsPb, CsSn, KPb, KSn, RbPb, and RbSn, but not NaPb), the B2 compounds LiAu and LiHg, the $L1_0$ compound NaBi, the oC16 compound NaHg, and the mC32 compound NaSi. In the sequence of alkali–gold compounds LiAu, NaAu, KAu, RbAu, and CsAu, one would similarly predict that the transition between metallic and insulating behavior occurs between NaAu and KAu.

It is important to emphasize that the ability to separate structures shown by the present orbital radii (Figs. 21–24) is far from being trivial or accidental. This can be demonstrated by constructing structural plots using different coordinates. We have used Miedema's (1973, 1976, Miedema *et al.*, 1975) coordinates $R_2 = |\phi_A^* - \phi_B^*|$ and $R_1 = |n_A^{*\frac{1}{3}} - n_B^{*\frac{1}{3}}|$, where ϕ_A^* and $n_A^{*\frac{1}{3}}$ are the effective elemental work function and cell boundary density to the power of $\frac{1}{3}$. Those coordinates were extremely successful in predicting the signs (and often the magnitudes) of the heats of formation of more than 500 compounds. We have also used a Mooser-Pearson (1959) plot, where R_2 is the elemental electronegativity difference, and R_1 is the average principal quantum number. Finally, we constructed a plot using Shaw's parameters, where R_2 is the elemental electronegativity difference and $R_1 = \frac{1}{2}(Z_A + Z_B)/[\frac{1}{2}(n_A + n_B)]^3$, where Z_A and n_A are the atomic number and the principal quantum number of the outer valence orbital, respectively.

In a Miedema plot, one notices a rough separation of the B1 and $B8_1$ structures (CsAu and RbAu appear, as in our case, at high $\Delta\phi^*$, $\Delta n^{*\frac{1}{3}}$), whereas most other structures are nearly indistinguishable. This illustrates the great difficulty in carrying the success of a theory that predicts *global binding energies* ΔE_0 into the prediction of *structural energies* ΔE_s (cf. Sec. I).

The Mooser-Pearson plot for these compounds appears visually as if only 104 compounds (i.e., isolated points) are plotted. In fact, it includes 360 compounds belonging to 14 different structures. This strong overlap of different structures on the same (R_1, R_2) coordinate reflects the insensitivity of the scale to separating such structures. A somewhat better separation is evident using Shaw's parameters, but the overlap of different structures is still extremely large.

It is likely that one could construct first-principles atomic pseudopotentials using somewhat different procedures than have been used here (Sec. III,A) for defining the pseudo wavefunctions. While this would result in a different set of orbital radii, they will most likely scale linearly with the present set of radii. Consequently, one may expect that the systematization of the crystal structures, based on such radii, will be essentially unchanged.

The relationship between the structural stability of a polyatomic system and the degree of repulsiveness of the effective atomic cores of the constituent atoms has been discussed in 1948 by Pitzer in a remarkable paper preceeding all pseudopotential theories. While one might have thought then naively that the electron-core attraction term $-Z_v/r$ would lead to a strong penetration by valence electrons of the core regions of neighboring atoms, Pitzer has realized that the core electrons set up a repulsive potential with a characteristic radius inside which such a penetration is discouraged. Hence, the triple bond energy of N≡N is much higher than that of P≡P (and the bond length in N≡N is significantly shorter than in P≡P) because the repulsive core size of nitrogen is so much smaller than that of phosphorous. Similarly, the occurance of multiple chemical bonds with first row elements as compared with the rare occurance of such bonds (with a small bond energy) with heavier atoms has been naturally explained in terms of the large repulsive core size of the latter elements. In addition, Pitzer noted that whereas Pauling (e.g., 1960) has suggested that single bond energies (e.g., N—N) should be roughly $\frac{3}{4}$ of the tetrahedral bond energy (e.g., C—C), in fact the ratio of the two is closer to $\frac{1}{2}$. This discrepancy was simply explained (Pitzer, 1948) by the fact that the change from the bond angle of 90° characteristic of p-type single bonds to a tetrahedral angle of 109.5° minimized in the latter case their overlap with the repulsive core.

In the present orbital radii approach, these ideas are realized in a simple manner. To first order, the change in energy per atom introduced by incorporating an atom in a polyatomic system is proportional to:

$$\delta E \sim \sum_l k_l \int \Delta\rho_l(r)[U_l(r) + \Delta(r)]\, dr \tag{24}$$

where $\Delta\rho_l$ is the lth component of the charge redistribution, $U_l(r)$ is the Pauli repulsive potential [Eq. (10)], $\Delta(r)$ the l-independent part of the atomic pseudopotential [Eq. (9)] and k_l are constants. The first $\Delta\rho_l(r)U_l(r)$ term in Eq. (24) leads to a repulsive and angular-momentum dependent contribution (for electron-attracting species) while the second term is isotropically attractive (for similar atoms). Neglecting, for this simple argument, the nonlinear dependence of the charge density redistribution $\Delta\rho_l(r)$ on $U_l(r)$, one notes that Pitzer's ideas on the destabilizing role of large-core atoms—as

well as the relative stability of structures that minimize such repulsions through conformational changes in bond angles—are directly manifested in Eq. (24). One could further note that charge redistribution effects occuring predominantly outside the pseudopotential core [where $U_l(r) \approx 0$] do not contribute to such strongly directional repulsive terms. It would seem reasonable that the dominance of the centrifugal barrier at small distances form the origin will cause the charge redistribution effects in the high angular momentum components of the density to be confined to regions outside U_l (i.e., $r \gtrsim r_l$). This simple picture clearly indicates the important structural role played by the r_s and r_p coordinates, as compared to higher angular-momentum orbital coordinates.

VI. SUMMARY

It has been demonstrated that the pseudopotential theory in its present nonempirical density-functional form is capable of providing transferable atomic pseudopotentials $v_{ps}^{(l)}(r)$ that can be used both for performing reliable quantum-mechanical electronic structure calculations and for defining semi-classical-like elementary length and energy scales. The resulting radii correlate with a large number of classical constructs that have been traditionally used to systematize structural and chemical properties of many systems.

At the same time, the orbital radii derived here are capable of predicting the stable crystal structure of the 112 octet compounds (Fig. 21), 419 suboctet compounds (Figs. 22–23) and the 34 superoctet compounds (in Fig. 24) with a remarkable success, exceeding 95%. The compounds for which the present theory does not predict the correct crystal structure are analyzed and found to be largely characterized as defect structures with many unusual electronic, magnetic and structural properties. Although I am unable at this time to provide a direct *causal* quantum-mechanical model explaining this remarkable success, I am hopeful that the use of these concepts in solving practical crystallographic, metallurgical, and chemical problems may be useful and will also eventually provide the insight needed for a microscopic theory elucidating the success of the orbital radii.

ACKNOWLEDGMENTS

I would like to thank A. N. Bloch, M. L. Cohen, and J. C. Phillips for inspiring discussions. Special thanks are due to E. Parthé and F. Hulliger for reviewing the present compliation of crystal structures. I am grateful to L. Pauling for bringing Pitzer's work (1948) to my attention and discussing related work.

REFERENCES

Abarenkov, J. V., and Heine, V. (1965). *Philos. Mag.* [8] **12**, 529.
Amand, R., and Glessen, B. C. (1978). *Scr. Metall.* **12**, 1021.
Andreoni, W., Baldereschi, A., Meloni, F., and Phillips, J. C. (1978). *Solid State Commun.* **24**, 245.
Andreoni, W., Baldereschi, A., Biemont, E., and Phillips, J. C. (1979). *Phys. Rev. B* **20**, 4814.
Appelbaum, J. A., and Hamann, D. R. (1976). *Rev. Mod. Phys.* **48**, 3.
Ashcroft, N. W. (1966). *Phys. Lett.* **23**, 48.
Ashcroft, N. W. (1968). *J. Phys. C* **1**, 232.
Ashcroft, N. W., and Langreth, D. C. (1967). *Phys. Rev.* **159**, 500.
Barber, M., Linnett, J. W., and Taylor, M. (1961). *J. Chem. Soc.* p. 3323.
Bennett, B. I., and Vosko, S. H. (1972). *Phys. Rev. B* **6**, 7119.
Bertoni, C. M., Bortolani, V., Calandra, C., and Nizzoli, E. (1973). *J. Phys. F* **3**, L244.
Best, K. J., Rodies, H. J., and Jacobi, H. (1971). *Z. Mettallkd.* **62**, 634.
Bose, A., Frohberg, G., and Wever, H. (1979). *Phys. Status Solidi A* **52**, 509.
Bras, J., Couderc, J. J., Fagot, M., and Ferre, J. (1977). *Acta Metall.* **25**, 1077.
Brewer, L. (1963). *In* "Electronic Structure and Alloy Chemistry of the Transition Elements" (P. Beck, ed.). Wiley (Interscience), New York.
Brewer, L. (1967). *In* "Phase Stability in Metals and Alloys" (P. Rudman, J. Stringer, and R. I. Jaffee, eds.), p. 39. McGraw-Hill, New York.
Brewer, L. (1968). *Science* **161**, 115.
Brewer, L., and Wengert, P. R. (1973). *Metall. Trans.* **4**, 2674.
Brodsky, M. B., and Brittain, J. O. (1969). *J. Appl. Phys.* **40**, 3615.
Brust, D. (1968). *Methods Comput. Phys.* **8**, 33.
Caskey, G. R., Franz, J. M., and Sellmyer, D. J. (1972). *J. Chem. Solids* **34**, 1179.
Chelikowsky, J. R., and Cohen, M. L. (1976). *Phys. Rev. B* **14**, 556.
Chelikowsky, J. R., and Phillips, J. C. (1978). *Phys. Rev. B* **17**, 2453.
Clementi, E., and Roetti, C. (1974). *At. Data Nuc. Data Tables* **14**, 1974.
Cohen, M. L., and Bergstresser, T. K. (1966). *Phys. Rev.* **141**, 739.
Cohen, M. L., and Heine, V. (1961). *Phys. Rev.* **122**, 1821.
Cohen, M. L., and Heine, V. (1970). *Solid State Phys.* **24**, 38.
Darken, L. S., and Gurry, R. W. (1953). "Physical Chemistry of Metals." McGraw-Hill, New York.
Elliot, R. P. (1965). "Constitution of Binary Alloys," 1st Suppl. McGraw-Hill, New York.
Engle, N. (1939). *Ingenioren* M101.
Engel, N. (1967). *Acta Metall.* **15**, 557.
Fock, V., Vesselow, M., and Petraschen, M. (1940). *Zh. Eksp. Teor. Fiz.* **10**, 723.
Friedel, J. (1969). *In* "The Physics of Metals" (J. M. Ziman, ed.) p. 1. Cambridge Univ. Press, London and New York.
Gerold V. (1978). *J. Appl. Crystallogr.* **11**, 153.
Goldman, A. (1977), *Phys. Status Solidi B* **81**, 9.
Gombas, P. (1935). *Z. Phys.* **94**, 473.
Gombas, P. (1967). "Pseudopotentials." Springer, Vienna (and references therein).
Gordy, W. (1946). *Phys. Rev.* **69**, 604.
Hafner, J. (1978). *Solid State Commun.* **27**, 263.
Hamann, D. R. (1979). *Phys. Rev. Lett.* **42**, 662.
Hamann, D. R., Schlüter, M., and Chiang, C. (1980). *Phys. Rev. Lett.* **43**, 1494.
Hansen, P. M. (1958). "Constitution of Binary Alloys." McGraw-Hill, New York.
Harris, J., and Jones, R. O. (1978). *Phys. Rev. Lett.* **41**, 191.

Harrison, W. A. (1966). "Pseudopotentials in the Theory of Metals." Benjamin, New York.
Hasegawa, A., and Watabe, M. (1977). *J. Phys. F* **7**, 75.
Hellman, H. (1935a). *J. Chem. Phys.* **3**, 61.
Hellman, H. (1935b). *Acta Physicochim. URSS* **1**, 913.
Hellman, H. and Kassatotschikin, W. (1936). *J. Chem. Phys.* **4**, 324.
Herget, R., Wreser, E., Gengnagel, H., and Gladun, A. (1970). *Phys. Status Solidi* **41**, 255.
Hewaidy, I. F., Busmann, E., and Klein, W. (1964). *Z. Anorg. Allg. Chem.* **328**, 283.
Hodges, C. H. (1977). *J. Phys. C* **7**, L247.
Hohenberg, P. C., and Kohn, W. (1964). *Phys. Rev.* **136**, 864.
Honke, D., and Parthé, E. (1965). *Acta Crystallogr.* **20**, 572.
Huffman, G. P. (1971). *J. Appl. Phys.* **42**, 1606.
Hultgren, R., Desai, R. D., Hawkins, D. T., Gleiser, H. G., and Kelley, K. K. (1973). "Selected Values of the Thermodynamic Properties of Binary Alloys." Am. Soc. Metals, Metals Park, Ohio.
Hume-Rothery, W., and Raynor, G. V. (1954). "The Structure of Metals and Alloys." Institute of Metals, London.
Kahn, L. R., Baybutt, P., and Truhlar, D. G. (1976). *J. Chem. Phys.* **65**, 3826.
Kerker, G. P. (1980). *J. Phys. C* **13**, L189.
Kerker, G. P., Zunger, A., Cohen, M. L., and Schlüter, M. (1979). *Solid State Commun.* **32**, 309.
Kiewit, D. A., and Brittain, J. O. (1970). *J. Appl. Phys.* **41**, 710.
Kohn, W., and Sham, L. J. (1965). *Phys. Rev.* **140**, 1133.
Kubaschewski, O., and Alcock, C. B. (1979). "Metallurgical Thermochemistry," 5th ed. Pergamon Oxford.
Lam, P., Cohen, M. L., and Zunger, A. (1980). *Phys. Rev. B* **22**, 1698.
Landolt-Börnstein (1971). *In* "Structure Data of Elements and Intermetallic Phases" (K. H. Hellwege and A. M. Hellwege, eds.), New Ser., Vol. 6. Springer-Verlag, Berlin and New York.
Littlewood, P. (1980). *J. Phys. C* **12**, 4441.
Machlin, E. S., Chow, T. P., and Phillips, J. C. (1977). *Phys. Rev. Lett.* **38**, 1292.
Marsh, R. E., and Shoemaker, D. P. (1953). *Acta Crystallogr.* **6**, 197.
Meisel, M. W., Helperin, W. P., Ochiani, Y., and Brittain, J. O. (1978). *J. Phys. F* **10**, 1105.
Miedema, A. R. (1973). *J. Less-Common Met.* **32**, 117.
Miedema, A. R. (1976). *J. Less-Common Met.* **46**, 67.
Miedema, A. R., Boom R., and De Boer, F. R. (1975). *J. Less-Common. Met.* **41**, 283.
Moore, C. E. (1971). "Atomic Energy Levels," NSRDS-NBS, Vols. 34–35. US Gov. Printing Office, Washington, D.C.
Mooser, E., and Pearson, W. B. (1959). *Acta Crystallogr.* **12**, 1015.
Moruzzi, V. L., Janak, J. F., and Williams, A. R. (1978). "Calculated Electronic Properties of Metals." Pergamon, Oxford.
Müller, C., Seifert, G., Lautenschläger, G., Wonn, H., Ziesche, P., and Mrosan, E. J. (1979). *Phys. Status Solidi B* **91**, 605.
Natapoff, M. (1975). *J. Phys. Chem. Solids* **36**, 53.
Natapoff, M. (1976). *J. Phys. Chem. Solids* **37**, 59.
Natapoff, M. (1978). *J. Phys. Chem. Solids* **39**, 1119.
Navrotsky, A., and Phillips, J. C. (1975). *Phys. Rev. B* **11**, 1583.
Pandey, K. C., and Phillips, J. C. (1974). *Phys. Rev. B* **9**, 1552.
Parthé, E. (1964). "Crystal Chemistry of Tetrahedral Structures." Gordon & Breach, New York.
Pauling, L. (1960). "The Nature of the Chemical Bond." Cornell Univ. Press, Ithaca, New York.
Pawley, G. S. (1968). *Acta Crystallogr., Sect. B* **24**, 485.
Pearson, W. B. (1967). "A Handbook of Lattice Spacings and Structures of Metals and Alloys," Vols. 1 and 2. Pergamon, Oxford.

Pearson, W. B. (1969). *In* "Development in the Structural Chemistry of Alloy Phases" (B. C. Giessen, ed.), p. 1. Plenum, New York.
Pearson, W. B. (1972). "The Crystal Chemistry and Physics of Metal Alloys." Wiley (Interscience), New York.
Pettifor, D. G. (1979). *Phys. Rev. Lett.* **42**, 846.
Phillips, J. C. (1970). *Rev. Mod. Phys.* **42**, 317.
Phillips, J. C. (1973). "Bonds and Bands in Semiconductors." Academic Press, New York.
Phillips, J. C. (1977). *Solid State Commun.* **22**, 549.
Phillips, J. C. (1978). *Comments Solid State Phys.* **9**, 11.
Phillips, J. C., and Kleinman, L. (1959). *Phys. Rev.* **116**, 287.
Phillips, J. C., and Van Vechten, J. A. (1970). *Phys. Rev. B* **2**, 2147.
Pitzer K. S. (1948). *J. Am. Chem. Soc.* **70**, 2148.
Redondo, A., Goddard, W. A., and McGill, T. C. (1977). *Phys. Rev.* **15**, 5038.
Rieger, W., and Parthé, E.. (1966). *Acta Crystallogr.* **22**, 919.
Rudman, P. S., Stringer, J., and Jaffe, R. I. (1966). "Phase Stability in Metals and Alloys." McGraw-Hill, New York.
St. John, J., and Bloch, A. N. (1974). *Phys. Rev. Lett.* **33**, 1095.
Schaefer, H. F., ed. (1977a). "Methods of Electronic Structure Theory." Plenum, New York.
Schaefer, H. F., ed. (1977b). "Application of Electronic Structure Theory." Plenum, New York.
Schlüter, M., Zunger, A., Kerker, G. P., Ho, K. M., and Cohen, M. L. (1979). *Phys. Rev. Lett.* **42**, 540.
Schob, O., and Parthé, E. (1964). *Acta Crystallogr.* **19**, 214.
Schubert, K. (1964). "Kristallstrukturen Zweikomponentiger Phasen." Springer-Verlag, Berlin and New York.
Schubert, K. (1977). *In* "Intermetallic Compounds" (J. H. Westbrook, ed.), p. 100. Robert E. Krieger Publ. Co., Huntington, New York.
Schubert, K., and Eslinger, P. (1957). *Z. Metallkd.* **48**, 126, 193.
Sellmyer, D. J., Caskey, G. R., and Franz, J. (1971). *J. Phys. Chem. Solids* **33**, 561.
Shannon, R. D., and Prewitt, C. T. (1969). *Acta Crystallogr., Sect. B* **25**, 925.
Shaw, R. W. (1968). *Phys. Rev.* **174**, 769.
Shunk F. A. (1969). "Constitution of Binary Alloys," 2nd Suppl. McGraw-Hill, New York.
Simons, G. (1971a). *J. Chem. Phys.* **55**, 756.
Simons, G. (1971b). *Chem. Phys. Lett.* **12**, 404.
Simons, G., and Bloch, A. N. (1973). *Phys. Rev. B* **7**, 2754.
Slater, J. C. (1956). "Theory of Alloy Phases," pp. 1–12. Am. Soc. Metals, Cleveland, Ohio.
Slater, J. C. (1974). "The Self-Consistent Field for Molecules and Solids," Vol. 4, p. 94. McGraw-Hill, New York.
Spicer, W. E. (1962). *Phys. Rev.* **125**, 1297.
Stroud, D., and Ashcroft, N. W. (1971). *J. Phys. F* **1**, 113.
Szasz, L., and McGinn, G. (1967). *J. Chem. Phys.* **47**, 3495.
Topiol, S., Zunger, A., and Ratner, M. (1977). *Chem. Phys. Lett.* **49**, 367.
Varma, C. M. (1979). *Solid State Commun.* **31**, 295.
Walter, J. P., Fong, C. Y., and Cohen, M. L. (1973). *Solid State Commun.* **12**, 303.
Warshel, A. (1977). *In* "Semiempirical Methods of Electronic Structure Calculations" (G. A. Segal, ed.), p. 133. Plenum, New York.
Wertheim, G. K., and Wernick, J. H. (1967). *Acta Metall.* **15**, 297.
Wykoff, R. W. G. (1963). "Crystal Structures," 2nd ed., Vols. 1–3. Wiley (Interscience), New York.
Yang, Y. W., and Coppens, P. (1974). *Solid State Commun.* **15**, 1555.
Zunger, A. (1979). *J. Vac. Sci. Technol.* **16**, 1337.
Zunger, A. (1980a). *Phys. Rev. B* **22**, 649.

Zunger, A. (1980b). *Phys. Rev. B* **22**, 959.
Zunger, A. (1980c). *Phys. Rev. B* **21**, 4785.
Zunger, A. (1980d). *Phys. Rev. Lett.* **44**, 582.
Zunger, A., and Cohen, M. L. (1978a). *Phys. Rev. Lett.* **41**, 53.
Zunger, A., and Cohen, M. L. (1978b). *Phys. Rev. B* **18**, 5449.
Zunger, A., and Ratner, M. (1978). *Chem. Phys.* **30**, 423.
Zunger, A., and Cohen, M. L. (1979a). *Phys. Rev. B* **19**, 568.
Zunger, A., and Cohen, M. L. (1979b). *Phys. Rev. B* **20**, 4082.
Zunger, A., Kerker, G. P., and Cohen, M. L. (1979a) *Phys. Rev. B* **20**, 581.
Zunger, A., Topiol, S., and Ratner, M. (1979b). *Chem. Phys.* **39**, 75.
Zunger, A., Perdew, J. P., and Oliver, G. (1980). *Solid State Commun.* **34**, 933.